Title: Heterogeneity of Radial Glia-Like Cells in the Adult Hippocampus.
Authors: Gebara E, Bonaguidi MA, Beckervordersandforth R, Sultan S, Udry F, Gijs PJ, Lie DC, Ming GL, Song H, Toni N
Journal: Stem cells (Dayton, Ohio)
Year: 2016 Apr
Volume: 34
Issue: 4
Pages: 997-1010
DOI: 10.1002/stem.2266

Title: "Heterogeneity of radial glia-like cells in the adult hippocampus"

Authors:

Elias Gebara[1], Michael Anthony Bonaguidi[2,4#], Ruth Beckervordersandforth[3#], Sébastien Sultan[1], Florian Udry[1], Pieter-Jan Gijs[1], Dieter Chichung Lie[3], Guo-li Ming[4,5,6], Hongjun Song[4,5,6] and Nicolas Toni[1]

[1]Department of Fundamental Neuroscience, University of Lausanne, 9, rue du Bugnon, 1005 Lausanne, Switzerland
[2] Current address: Eli and Broad CIRM Center for regenerative Medicine and Stem Cell Research, University of Southern California, 1425 San Pablo Street, Los Angeles, CA 90033, USA.
[3] Institute of Biochemistry, Friedrich-Alexander Universität, Erlangen-Nürnberg, Fahrstrasse 17, 91054 Erlangen, Germany
[4] Institute for Cell Engineering, [5]Department of Neurology, [6]The Solomon Snyder Department of Neuroscience, Johns Hopkins University School of Medicine, Baltimore, MD 21205, USA
# Equally contributing authors

Author contributions:

N.T., E.G., conceived and designed the experiments. E.G., MA.B., R.B., S.S., F.U. and PJ.G. performed the experiments. E.G. analyzed the data. E.G., MA.B., R.B., S.S., DC.L, H.J. and N.T discussed the data. E.G. and N.T. wrote the manuscript. N.T., GL.M, H.S. provided financial support.

Corresponding author:

Nicolas Toni, PhD
9, rue du Bugnon,
1005 Lausanne, Switzerland
Phone : ++4121-692-5133
Email: Nicolas.toni@unil.ch

Abstract

Adult neurogenesis is tightly regulated by the neurogenic niche. Cellular contacts between niche cells and neural stem cells are hypothesized to regulate stem cell proliferation or lineage choice. However, the structure of adult neural stem cells and the contact they form with niche cells are poorly-described.

Here, we characterized the morphology of radial glia-like (RGL) cells, their molecular identity, proliferative activity and fate determination in the adult mouse hippocampus. We found the co-existence of two morphotypes of cells with prototypical morphological characteristics of RGL stem cells: Type α cells, which represented 76% of all RGL cells, displayed a long primary process modestly branching into the molecular layer and type β cells, which represented 24% of all RGL cells, with a shorter radial process highly branching into the outer granule cell layer-inner molecular layer border. Stem cell markers were expressed in type α cells and co-expressed with astrocytic markers in type β cells. Consistently, *in vivo* lineage tracing indicated that type α cells can give rise to neurons, astrocytes and type β cells, whereas type β cells do not proliferate.

Our results reveal that the adult subgranular zone of the dentate gyrus harbors two functionally different RGL cells, which can be distinguished by simple morphological criteria, supporting a morpho-functional role of their thin cellular processes. Type β cells may represent an intermediate state in the transformation of type α, RGL stem cells, into astrocytes.

Introduction

The adult mammalian brain retains neural stem cells in two discrete areas, the subventricular zone and dentate gyrus of the hippocampus[1, 2]. Increasing evidence suggests that upon maturation, new neurons are involved in mechanisms of learning and indeed, the stimulation of adult hippocampal neurogenesis increases learning and memory performances[3, 4]. Thus, mechanisms involved in the regulation of adult neurogenesis are of great interest for our understanding of learning and memory and for the potential treatment of memory impairment.

In the hippocampus, adult neural stem cells reside in the subgranular zone of the dentate gyrus and may display a radial glia-like (RGL) morphology. They are characterized by a long process that extends through the granule cell layer (GCL) and widely branches in the outer GCL and in the inner third of the molecular layer[5-8]. Adult neural stem cells in the subgranular zone may also display shorter, horizontal processes[9, 10] greater proliferative activity than RGL stem cells[11], suggesting the existence of a morpho-functional component in the regulation of quiescence.

During embryonic development, time-lapse imaging showed that RGL stem cells generate neurons which use their parent cell's radial process to migrate to the cortical plate, a mechanism that may underlie the radial organization of the neocortex[12]. In adult neurogenesis however, the function of the radial process in RGL stem cells is not clearly defined. Although the primary process is often seen alongside dendrites from nascent neurons[13], it is unclear whether it is used for the migration of the newborn neurons or for establishing contacts with the neurogenic niche. Furthermore, clonal analysis suggested that newly-formed neurons in the adult hippocampus migrate away from their parent cells[14] and may use the vasculature for a tangential migration [15]. Thus, a potential function of the radial processes of adult RGL stem cells may rather be found in regulating their proliferation or fate through interactions with the local niche[16].

The direct cellular environment of neural stem cells plays a fundamental role in the regulation of adult neurogenesis. Indeed, although proliferating cells reside in the entire central nervous system, adult neurogenesis is restricted to the hippocampus and the subventricular zone.

However, when transplanted in the hippocampus, progenitor cells from a non-neurogenic area such as the spinal cord regain the ability to generate neurons and inversely, when transplanted in a non-neurogenic area, hippocampal neural stem cells lose their ability to differentiate into neurons[17]. This indicates that the intrinsic neurogenic potential of central nervous system progenitor cells is controlled by the neurogenic niche.
Several cell types of the neurogenic niche have been shown to play a role in the regulation of the neural stem cell proliferation, including endothelial cells[18], astrocytes[19, 20], neurons[21] or microglia[22, 23]. The effect of niche cells on stem cells may be mediated by the release of soluble molecules such as Wnt3a[19] or GABA[21] or by direct contact such as with microglia[23] or astrocytes[24]. These observations suggest that the complex morphology of RGL stem cells enables the establishment of numerous contacts with a variety of cell types of the hilus, granule cell layer and molecular layer of the dentate gyrus, all of which may participate to its regulation.
The morphology of the RGL stem cells is still poorly-described and in particular, it is still unknown whether there is a structure-function relationship among the population of this highly morphologically variable population of cells. The goal of this study is to examine the fine structure of RGL stem cells in the adult hippocampal niche and to test the possibility that the morphological characteristics of RGL stem cells may reflect their function.

Materials and methods

Ethics statement
This study was carried out in strict accordance with the recommendations in the Guidance for the Care and Use of Laboratory Animals of the National Institutes of Health. All experimental protocols were approved by the Swiss animal experimentation authorities (Service de la consommation et des affaires vétérinaires, Chemin des Boveresses 155, 1066 Epalinges, Switzerland). Every effort was made to minimize the number of animals used and their suffering.

Experimental animals
Animals used for this study were adult male mice. GFAP-GFP mice were a kind gift from the laboratory of Helmut Kettenmann (Max-Delbruck center, Berlin, Germany)[25]. They express the green fluorescent protein (GFP) under the control of the human glial fibrillary acidic protein promoter (GFAP). Nestin-GFP mice were a kind gift from the laboratory of K. Mori (PRESTO, Kyoto, Japan)[26]. These mice express the green fluorescent protein (GFP) under the stem cell-specific promoter Nestin. Nestin::CreER^{T2} and Z/EG$^{f/+}$ mice were purchased from The Jackson Laboratory (Maine, USA). The Rosa26tdTomato reporter mice[27] were a kind gift from the laboratory of Jean-Yves Chatton (Department of Fundamental Neurosciences, University of Lausanne, Switzerland). The GFAP::CreER^{T2}-Rosa YFP were a kind gift from the laboratory of Andrea Volterra (Department of Fundamental Neurosciences, University of Lausanne, Switzerland).
For clonal analysis, we used the GFAP::CreER^{T2} and the Nestin::CreER^{T2} mice. The Nestin::CreER^{T2} mice were crossed with fluorescent reporter mice Rosa-tdTomato or Z/EG$^{f/+}$. Tamoxifen (62 mg/ml; Sigma; T5648) was prepared in a 5:1 ratio of corn oil to ethanol at 37°C with occasional vortexing. A single tamoxifen or vehicle dose was injected into 8–10 week-old mice (i.p. 62 mg/kg) for Nestin::CreER^{T2}-Z/EG$^{f/+}$ mice, 60 mg/kg for Nestin::CreER^{T2}-Rosa26tdtomato mice or 86 mg/kg for the GFAP::CreER^{T2}-RosaYFP mice.
For exercise and aging experiments, young adult mice were 6-week-old and aged mice were 7.5-month-old at the beginning of the experiment. Runner mice were housed for 2 weeks in

standard cages with free access to a running wheel (Fast-Trac; Bio-Serv, USA). Non-runner mice were housed in similar, adjacent cages without running wheel. All mice were housed in a 12-h light/dark cycle and controlled temperature of 22 °C. Food and water were available *ad libitum*.

BrdU and D-serine administration
All mice were injected intraperitoneally with the thymidine analog Bromodeoxyuridine (BrdU, Sigma-Aldrich, Buchs, Switzerland), at doses of 100 mg/kg in saline. D-serine was prepared fresh every day and diluted in water containing 0.9% NaCl. 7 week-old mice were injected intraperitoneally every day with 50 mg/kg of D-serine (Sigma-Aldrich) for 8 consecutive days or with the same volume of vehicle (0.9% NaCl in water).

Tissue collection and preparation
At the end of the experiment, mice received a lethal dose of pentobarbital (10mL/kg, Sigma-Aldrich, Buchs, Switzerland) and were perfusion-fixed with 50 ml of 0.9% saline followed by 100mL of 4% paraformaldehyde (Sigma-Aldrich, Switzerland) dissolved in phosphate buffer saline (PBS 0.1M, pH 7.4). Brains were then collected, postfixed overnight at 4°C, cryoprotected 24h in 30% sucrose and rapidly frozen. Coronal frozen sections of a thickness of 40 µm (50 µm for clonal analysis) were cut with a microtome-cryostat (Leica MC 3050S) and slices were kept in cryoprotectant (30% ethylene glycol and 25% glycerin in 1X PBS) at -20°C until processed for immunostaining.

Immunohistochemistry
Immunochemistry was performed on 1-in-6 series of section. Sections were washed 3 times in PBS 0.1M. BrdU detection required a DNA denaturation for 20 min in 2 M HCl at 37°C and rinsed in 0.1 M borate buffer pH 8.5 for 15 min. Then, slices were incubated in blocking solution containing 0.3% Triton-X100 and 15% normal serum (normal goat serum (Gibco) or normal donkey serum (Sigma Aldrich), depending on the secondary antibody) in PBS 0.1M. Slices were then incubated 40 hours at 4°C with the following primary antibodies: Chicken anti-GFP (1:500, AnaSpec Inc), Rabbit anti-GFP (1:500, AnaSpec Inc), mouse monoclonal anti-BrdU (1:250, Chemicon International), rabbit anti-K-i67 (1:200, Abcam), rabbit anti-Sox1 (1:500, Abcam), rabbit anti-GFAP (1:500, Invitrogen), goat anti-Iba1 (1:200, Abcam), rabbit anti-Sox2 (1:500, Millipore), rabbit anti-NG2 (1:400, Chemicon) mouse anti-CD133 (Prominin 1, 1:500, Millipore), mouse anti-Nestin (1:200, Millipore), rabbit anti-S100B (1:500, Abcam), rabbit anti-GLT1 (1:500, Abcam). The sections were then incubated for 2 hours in either of the following secondary antibodies: Dylight 488 goat anti-chicken (1:500, Jackson ImmunoResearch), goat anti-rabbit Alexa-488 (1:250, Invitrogen) goat anti-mouse Alexa-594 (1:250, Invitrogen), goat anti-rabbit Alexa-594 (1:250, Invitrogen), donkey anti-goat Alexa-555 (1:250, Invitrogen), donkey anti-rabbit Alexa 647 (1:250, Invitrogen). Blood vessels were labeled by Sulforhodamine 101 (Invitrogen). 4,6 diamidino-2-phenylindole (Dapi) was used to reveal nuclei.

Image analysis
Images were collected with a Zeiss confocal microscope (Zeiss LSM 710 Quasar Carl Zeiss, Oberkochen, Germany) and cell counts were performed using stereology principles, as previously described[28]. Briefly, for each animal, a 1-in-6 series of section between -1.3 to -2.9 mm from the Bregma was stained with the nucleus marker DAPI and used to measure the volume of the granule cell layer. The granule cell area was traced using Axiovision (Zeiss, Germany) software and the granule cell reference volume was determined by multiplying the area of the granule cell layer by the distance between the sections sampled (240 µm). All cells

were counted in the entire thickness of the sections in a 1-in-6 series of section (240 µm apart) with a 40x objective. All cells were counted blind with regard to the mouse status. The number of immunolabeled cells was then related to granule cell layer sectional volume and multiplied by the reference volume to estimate the total number of immunolabeled cells. RGL cells were counted in the sub-granular zone SGZ of the dentate gyrus.
Clones were analyzed as described in Bonaguidi et al, Cell 2011. Briefly, the tamoxifen dose was calibrated for each mouse line, so as to obtain a maximum of 4 clones per hippocampus. Clonal relation was then assessed within a distance of 150 µm from the type α RGL cell. Since progenies do not migrate more than 125 µm from the mother cell (as observed 2 months after tamoxifen injection in Bonaguidi et al, Cell 2011, Figure 1F), this distance is sufficient to guarantee more than 90% probability as a clone.

Statistical analysis:
Hypothesis testing was two-tailed. All analyses were performed using JMP10 software. First, Shapiro-Wilk tests were performed on each group of data to test for distribution normality. For normal distribution we performed parametric tests. When the distribution was not normal, a non-parametric Kruskal-Wallis test was used. Homoscedasticity of variances was tested by Bartlett's test and adequate analysis of variance (ANOVA) was performed, followed by a post-hoc multiple comparisons procedure t-test with Bonferonni correction. For two sample comparisons, when the distribution was normal, the equality of variances of the groups was tested by a bilateral F-test and the adequate unpaired t-test was used. All data are presented as mean ± SEM.

Results

Morphometry identifies two subtypes of RGL cells with distinct molecular marker expression

RGL cells were identified using two common transgenic mouse lines: the GFAP-GFP mice[25] and the Nestin-GFP mice[26]. In these mice, the Green Fluorescent Protein (GFP) is expressed under the control of the human Glial Fibrillary Acidic Protein (GFAP) promoter or the Nestin promoter, respectively. At 8 weeks of age, mice were prepared for histology and immunostaining against GFP was used to amplify the fluorescent signal. In both mice, GFP^+ RGL cells displayed a prototypical morphology, including a nucleus located in the subgranular zone of the DG, a radial process extending through the granule cell layer and extensively branching into the outer granule cell layer and the molecular layer and a few basal processes extending towards the hilus[5-8] (Figure 1A).
We measured the following parameters in 2472 GFAP-GFP^+ and 1150 Nestin-GFP^+ RGL cells: position of the soma relative to the basal limit of the granule cell layer, length of the primary process, number of secondary branches stemming from the primary process, projected surface of the territory encompassed by the whole cell or only by the secondary apical arbor and maximal width of the territory covered by the apical arbor (Figure 1, Supplementary Figure 1A). On average, the soma of RGL cells was found within 3.83 ± 0.07 µm of the base of the granule cell layer. The length of their primary radial process was 75.82 ± 0.34 µm; the main process had 4.11 ± 0.03 branches; the secondary dendritic tree had a width of 25.14 ± 0.11 µm, covered a projected surface of 569.51 ± 36.83 μm^2 and the whole cell covered a surface area of 1485.75 ± 17.99 μm^2. There was no inter-strain difference in the morphology of RGL cells, indicating that these parameters did not depend on the genetic background or the reporter, but rather reflected common features of RGL cells. Notably, there was a great variation in both the length and the width among RGL cells, which defined two

distinct populations: A first group of cells, which we named type α, represented 75.46 % of all RGL cells (73.8% in Nestin-GFP mice and 76.2% in GFAP-GFP mice). They displayed a long radial process and a narrow arbor of secondary processes, which extended beyond the granule cell layer, into the first third of the molecular layer. In contrast, a second group of cells named type β, which represented 24.54% of all RGL cells (26.2% in Nestin-GFP mice and 23.8% in GFAP-GFP mice), displayed a short primary process (shorter than 58 µm) and a broad arbor of secondary processes, most of which did not extend beyond the limit of the granule cell layer (Figure 1A-C). Due to their broader arbor of processes, type β cells displayed an increased projected surface of their apical arbor (Figure 1D-E). Type α and β cells were however similar in all other morphological criteria observed, regardless of the reporter mouse used to examine their morphology (Figure 1F-K). Thus, RGL cells are morphologically heterogeneous and are composed of 2 major morphotypes that can be clearly identified by the length of the primary process and the width of the arbor formed by the secondary processes.

We next examined the molecular identity of these two morphotypes using immunohistochemistry (Figure 2, Supplementary Figure 1B). All type α and β cells expressed the neural stem cell markers GFAP and Sox2. However, although the stem cell markers Sox1, Prominin 1 and Nestin were expressed in 100% of type α cells, they were only expressed in a fraction of type β cells (49%, 32%, 18% respectively). Inversely, the astrocyte-specific glutamate transporter GLT1 and calcium binding protein S100β were expressed by all and virtually only type β cells. This indicates that a fraction of β cells co-expressed astrocytes-specific (GLT1, S100β) and stem cell-specific markers (Prominin1, Nestin, Sox1). Intriguingly, the morphology of type β cells expressing Sox1, Prominin1 or Nestin was different than from immunonegative type β cells: Sox1, Prominin1 and Nestin were present in the cells with the longest processes, indicating that the length of the process was associated with a "stem-like" molecular identity of these cells (Figure 2E-J).

Thus, type α and type β cells can be characterized by morphology and molecular markers: While type α cells extend processes well into the molecular layer and express stem cell markers such as Sox2, Sox1, Nestin, GFAP and Prominin1, type β cells are restricted into the granule cell layer and express S100β and GLT1, accompanied by Prominin1, Sox1 and Nestin for the longest cells.

Cellular contacts with niche cells

The morphological differences between type α and type β cells may enable them to interact with distinct niche cells which, in turn, may underlie different regulation mechanisms of their activity. To examine the contacts between RGL cells and their cellular environment, as well as their relevance to proliferation, we examined mice in standard housing conditions and in cages containing a running wheel, a condition of voluntary exercise known to increase proliferation[4] (Figure 3). After two weeks of exposure to a running wheel (or the same housing cage without a running wheel), all mice were killed and immunohistochemistry was used to identify microglia (Iba1), astrocytes (S100β) and oligodendrocyte progenitor cells (NG2). Sulforhodamine 101 was used to identify blood vessels.

Under basal housing conditions (NR), individual RGL cell types contacted on average 2 blood vessels, 2.5 astrocytes, and 1.7 oligodendrocyte precursors, independently of their morphotype. In contrast, type β cells contacted significantly more microglia cells (2.8 microglia per type β cell) than by type α cells (1.6 microglia per type α cell, Figure 3B-I). The majority of the contacts with microglia occurred on the main process or the secondary processes of RGL cells, but no contact was observed on the soma (Figure 3B). In running conditions (R), both type α and type β cells contacted fewer microglia and more blood vessels than in non-running conditions. To test whether running affected RGL cells or niche cells, we

examined the morphology of niche cells in running conditions. Consistent with our previous observations[22], running decreased the number of Iba1-expressing microglia, but increased the size of their territory and the number of branches (Supplementary Figure 2A-C). Inversely, running increased the number and/or the size of blood vessels in the dentate gyrus, as reflected by increased number of pixels labeled by Sulforhodamine 101 (Supplementary Figure 2D-F).
These results indicate that type β cells preferentially contacted microglia and that voluntary running increased the number of blood vessels and decreased the number of microglia, therefore interfering with the contacts between type α and type β cells with the niche.

Type α and type β cells respond differently to pro-proliferative stimuli
The proliferation of adult neural stem/progenitor cells is regulated by external stimuli and is increased by voluntary running[4] and decreases with aging[29]. To examine whether these conditions affected the number or the morphology of type α and type β cells, 16 GFAP-GFP mice were divided in 4 experimental groups: young adult mice (8 weeks of age; Y) and older mice (8 months of age; O), that were housed individually in standard cages in presence (R) or absence (NR) of a running wheel for 2 weeks (Figure 4A, 4 mice per group). The total number of RGL cells was significantly decreased by aging and increased by running (Figure 4B, E). Similarly, voluntary running increased, whereas aging decreased the number of type α cells (Figure 4C). In contrast, neither running, nor aging had any effect on the total number of type β cells (Figure 4D). As a result, when the relative proportions of type α and type β cells were calculated, Y, YR and OR mice displayed mainly type α cells (66.6%, 80.6% and 58%, respectively), whereas type β cells were more frequently observed on O mice (89%, Figure 4B-E). The length and width of type α and type β cells were not modified by running or aging (Supplementary Figure 3). Thus, aging and exercise strongly modified the number of type α cells, but not the number of type β cells.
We next examined whether the pharmacological stimulation of adult neurogenesis cells may have a similar effect on the different morphotypes of cells. We recently reported that the administration of the NMDA receptor co-agonist D-serine increases the density of RGL stem cells[30]. Here, we repeated this experiment and injected four mice with D-serine (daily i.p. injections 50mg/kg, for 8 days during the eighth week of life) and four mice with the same volume of saline. All mice were examined 1 day after the last injection (Figure 5A). Similarly to our previous observations, D-serine increased the total number of RGL cells. This increase was mediated by an increase in both the number of type α cells (120% increase) and type β cells (160% increase, Figure 5B-E). Moreover, the effect of D-serine was specific to RGL cells, since D-serine treatment did not change the number of GFAP-immunolabeled stellar astrocytes in the dentate gyrus[30]. In order to examine whether D-serine activated the proliferation of type α and type β cells, we immunostained hippocampal slices for the cell proliferation marker Ki-67. Ki-67 is a nuclear protein associated with proliferation that is expressed during all active phases of the cell cycle. Out of 545 cells analyzed, Ki-67 was expressed in about 10.45% of type α cells, but was not expressed in type β cells (Figure 5F-G). D-serine significantly increased the proportion of Ki-67-expressing type α cells as compared to the proportion found in control, non-treated mice ($p<0.01$, Figure 6C).
Thus, D-serine increased the proliferation of type α and resulted in increased number of type α and type β cells, but did not affect the proliferation of type β cells.

Proliferative properties of type α and type β cells:
To examine the proliferative properties of type α and type β cells, we immunostained hippocampal slices for the cell proliferation marker Ki-67 (Figure 6A-C). Out of 1555 cells analyzed, Ki-67 was expressed in about 5% of type α cells, but was not expressed in type β

cells. Notably, type α-Ki-67^{+} cells displayed a longer process than type α-Ki-67^{-} cells (Figure 6D). These results suggest that type β cells do not proliferate and support the possibility that the RGL cells' processes may play a role in proliferation.

To further examine cell proliferation, we performed pulse chase experiments with three different BrdU injection protocols. By incorporating into the nascent DNA strand during mitosis, BrdU enables the labeling of dividing cells and their progenies. First, we injected mice with BrdU (1x 100 mg/kg) and sacrificed the mice 2 hours after the last BrdU-injection (Figure 6E). This protocol enables the labeling of fast dividing progenitor cells, however BrdU was incorporated in 3.9 % type α cells, but was absent from type β cells (Figure 6F). Then we injected mice with BrdU (3x 100 mg/kg) and sacrificed the mice 24 hours after the last BrdU-injection (Figure 6G-I). Out of 500 cells, BrdU was incorporated in 3.64% of type α and 0.4% of type β. Moreover, the BrdU^{+} type β cells were closely attached to BrdU^{+} type α cells (Figure 6H). In a third experiment, we injected mice with BrdU daily for 8 days (100 mg/kg) and sacrificed the mice one day after the last BrdU-injection (Figure 6J). Both type α and type β cell types incorporated BrdU, although type α cells to a much greater extent than type β cells (Figure 6K-L, 527 cells analyzed, BrdU^{+} type α: 5.69%, BrdU^{+} type β: 0.94%). In contrast with Ki-67 labeling, the proportion of BrdU-labeled cells did not correlate with the dimensions of the cells (Figure 6K).

Taken together, these results suggest that type β cells do not proliferate but are generated by the division of type α cells. To further examine this possibility, we performed a clonal analysis.

Fate analysis of type α and type β cells

To examine the fate of individual RGL cells, we used two transgenic mice, the GFAP::CreER^{T2} and the Nestin::CreER^{T2}. We crossed the Nestin::CreER^{T2} transgenic mouse (expressing the tamoxifen-inducible Cre recombinase under the control of the Nestin promoter) with reporter mice (ROSA-tdTomato or Z/EG$^{f/+}$) (Figure 7A). The GFAP::CreER^{T2} was crossed with the ROSA-YFP reporter mouse. A minimal tamoxifen injection resulted in the sparse labelling of adult neural stem cells, thereby enabling the identification and morphological analysis of individual clones[14]. In order to examine clones shortly after division, we sacrificed the animals 1, 2, 3 or 7 days after tamoxifen injection (dpi, Figure 7B). In Nestin::CreER^{T2} mice, we didn't detect any difference between the two reporter mice, therefore we combine the results of both mice. All clones are described and shown in Supplementary Figures 4-6. Across all time points, we examined 227 clones that contained at least one RGL cell, which were most frequently accompanied by a neuronal progenitor/type 2 cell (N) or an astrocyte (A, Figure 7 and Supplementary figure 4A). Astrocytes were defined by their typical stellar astrocytes morphology and their identity was confirmed by immunohistology against GFAP. Neuronal progenitor/type 2 cells were identified based on the absence of GFAP immunoreactivity and their short processes oriented horizontally or radially (Supplementary Figure 6). The most parsimonious clonal relationships between cells present in each clones revealed that 26.9% of the clones displayed an isolated RGL cell (all of which consisted of type α cells), suggesting no division, 37% of the clones divided once and 36.1% divided twice (Figure 7F-H, Supplementary figure 4A). Out of the 166 clones that divided at least once, 51.8 % generated a neural progenitor/type 2 cell, 24.7% generated an astrocyte and 77.7 % generated a RGL cell (including clones that contained neurons or astrocytes, Figure 7C). Type β cells were more often observed in clones that contained astrocytes than in clones containing neurons, suggesting that they originated from α cells that were prone to gliogenesis (Figure 7C). Finally, among the 129 clones in which a new RGL cell was observed, 44% generated 1 type β cell, 7% generated 2 type β cells and 49% generated a new type α cell (Figure 7D). Thus, out of 166 clones that divided at least once, 75

new type β cells and 63 new type α cells were generated (Figure 7E and see summary table on Supplementary Figure 5A).
In GFAP::CreER^{T2} mice, across all time points, we examined 93 clones. Similarly to Nestin::CreER^{T2} mice, 5.3% of the clones did not divide, 46.3 % divided once and 48.4% divided twice (supplementary figure 4B and supplementary Figure 5B). Out of the 88 clones that divided, 56.8 % generated a neuronal progenitor/type 2 cell, 12.5 % generated and astrocyte and 81.8 % generated a RGL cell. Moreover similarly to Nestin::Cre mice, type β cells were more often observed in clones that contained astrocytes.
Thus, type α cells undergo numerous modes of division to generate type α cells, type β cells, neurons and astrocytes and new type β cells are frequently generated upon division of type α cells.

Discussion

Using a combination of morphometry, immunohistochemistry and clonal analysis, we found that two morphotypes of RGL cells co-exist in the subgranular zone of the dentate gyrus, which can be characterized by two simple morphological features, the length of the primary process and the width of the arbor of secondary processes: Type α cells represented 76.21% of RGL cells and displayed a long radial process and a narrow arbor of secondary processes extending well into the first third of the molecular layer. These cells expressed stem cell markers, self-replicated and produced neurons, astrocytes and type β cells. Their total number was also greatly increased by voluntary running and D-serine administration and decreased by aging. In contrast, type β cells (which represented 23.79% of all RGL cells) had a short radial process and their secondary processes branched mainly in the granule cell layer. Marker expression analyses revealed the co-expression of astrocytic and stem cell markers. These cells did not proliferate and their population size did not change upon aging or exercise, but was increased by D-serine administration. Together, these results reveal the co-existence within the dentate gyrus, of two populations of cells with prototypical morphology of RGL stem cells, but with radically different morphological and functional properties.
The strong association between morphology and function of RGL cells suggests that the processes of RGL cells play a potential role in regulating their activity. The shorter processes of type β cells do not reach the molecular layer. Although the role of the highly-branched and long processes of RGL stem cells is still unclear, our results support the view that these processes establish specific contacts with the neurogenic niche[16]. We identified here that both type α and type β cells established direct cellular contacts with several cell types of the neurogenic niche, including but not restricted to microglia, astrocytes, NG2-expressing glia and blood vessels. Direct signaling with these cells are known to participate to the regulation stem cell proliferation and fate determination, as has recently been shown for astrocytes[24], blood vessels[18, 31], or microglia[22, 23]. Contacts with microglia seems of particular relevance to the identity of type β cells, since they contacted significantly more microglia than type α cells in normal (sedentary) conditions. The presence of microglia in the dentate gyrus has been associated with inflammation, which can reduce neurogenesis by the production of cytokines[32]. In absence of inflammation, microglia contribute to the phagocytosis of early progenitors undergoing apoptotic elimination during the neuroprogenitors to neuroblasts transition[23]. However, we found no evidence of microglial engulfment of type α or type β cells and the contacts that these cells established with microglia occurred mainly on the fine, secondary processes rather than on the soma, as has been described for phagocytic engulfment[23]. Our results therefore are consistent with the view that microglia may regulate RGL stem cell proliferation using paracrine or juxtacrine signaling, independently from

inflammatory pathway[22]. Consistently, running modified the number and the structure of microglia cells (Supplementary Figure 2) and resulted in increased proliferation of type α cells (Figure 3). Thus, cellular contacts established by RGL stem cells may be involved in the regulation of their proliferation. This possibility calls for a further examination of the specific contacts they form in the molecular layer, especially with microglia and blood vessels, with higher resolution imaging such as electron microscopy. Furthermore, whether the increased contacts between microglia and type β are a cause or consequence of their dormancy remains uncertain and this question will require further investigation with the use of live-cell imaging.

Type α cells display all characteristics of RGL stem cells[11, 14, 33, 34], but the identity of type β cells is less clear. Morphology and molecular marker expression suggest that these cells are intermediate between quiescent RGL stem cells and stellate, protoplasmic astrocytes. Indeed, type β cells express both stem cell markers such as Nestin, Prominin 1, Sox 1 and Sox 2, but also the mature astrocytic marker S100β and GLT1, which are normally not expressed in RGL stem cells[11]. Similarly, the morphology of type β cells is less polarized than type α cells, with shorter radial process and larger branches of secondary processes than type α cells, but not quite as round and branched as protoplasmic astrocytes. Furthermore, the absence of expression of the essential cell cycle marker Ki-67 from type β cells (Figure 6A-C), even upon activation by D-serine (Figure 5F-G) and the lack of BrdU incorporation in short (2h) pulses (Figure 6D-F) indicates that type β cells do not divide. Instead, we propose that type β cells are formed upon the division of type α cells. Consistent with this hypothesis, clonal analysis shows that type β cells were never found alone and all type β cells that incorporated BrdU after a 24 h pulse were found apposed to a type α cell (Figure 6G-I). Although we cannot exclude that type β cells may represent a highly-quiescent pool of RGL stem cells which may be converted into type α cells upon proper stimulation, this possibility is not supported by our results. Alternatively, type β cells may represent a transitional morphology of type α cells undergoing conversion into astrocytes, as has been proposed during aging[14, 33] or epilepsy-induced hyperactivation[35] (See schematic model in Supplementary Figure 7). In favor of this possibility, long primary processes in RGL cells were associated with Ki-67 expression (Figure 5F and 6D) and type β cells that expressed stem cell markers (Sox 1, Prominin 1 and Nestin), had a longer primary process than cells not expressing these markers (Figure 2). These correlations between marker expression and length of the primary process suggests the existence of a morphological continuum between RGL cells, with proliferation and the expression of stem cell markers decreasing with the shortening of the primary process. Intriguingly, the frequent production of type β cells upon division of type α cells does not result in an increase in the number of type β cells over time or in conditions of increased proliferation such as voluntary exercise. This apparent stability in the population of type β cells, together with the absence of microglia engulfment of type β cells also supports the idea of a stable turnover, in which type β cells may transform into astrocytes and migrate out of the granule cell layer. To maintain a stable population of type β cells under conditions of increased or decreased proliferation, the transformation into astrocytes would need to be regulated by the production of type β cells. Time-lapse imaging will shed light in the morphological dynamics and migratory pattern of type β cells.

Together, our results reveal the existence of two morpho-functionally distinct types of RGL cells in the adult dentate gyrus. The selective behavior of these cell types is relevant to the mechanisms of stem cell proliferation and self-renewal. Furthermore, the morphological criteria proposed here may be used to assess the status of the pool of RGL stem cells in the dentate gyrus.

Acknowledgments
The authors wish to thank the Cellular Imaging Facility of the University of Lausanne and Jacqueline Kocher-Braissant for technical help. This work was supported by the Swiss National Science Foundation (E.G., S.S., F.U. PJ.G and N.T), the Deutsche Forschungsgemeinschaft (DFG LI 858/9-1) and the Bavarian Research Network on Human induced Pluripotent Stem Cells "ForIPS" (D.C.L.), the Deutsche Forschungsgemeinschaft (BE5136/1-1) (R.B.), the NIH (NS048271 and MH105128) and Dr. Miriam and Sheldon G. Adelson Medical Research Foundation (G.-l.M.), NIH (NS047344; to H.S.),

References

1. Altman J, Das GD. Autoradiographic and histological evidence of postnatal hippocampal neurogenesis in rats. The Journal of comparative neurology. 1965;124:319-335.
2. Ming GL, Song H. Adult neurogenesis in the mammalian brain: significant answers and significant questions. Neuron. 2011;70:687-702.
3. Sahay A, Scobie KN, Hill AS, et al. Increasing adult hippocampal neurogenesis is sufficient to improve pattern separation. Nature. 2011;472:466-470.
4. van Praag H, Christie BR, Sejnowski TJ, et al. Running enhances neurogenesis, learning, and long-term potentiation in mice. Proceedings of the National Academy of Sciences of the United States of America. 1999;96:13427-13431.
5. Beckervordersandforth R, Deshpande A, Schaffner I, et al. In vivo targeting of adult neural stem cells in the dentate gyrus by a split-cre approach. Stem cell reports. 2014;2:153-162.
6. Huttmann K, Sadgrove M, Wallraff A, et al. Seizures preferentially stimulate proliferation of radial glia-like astrocytes in the adult dentate gyrus: functional and immunocytochemical analysis. The European journal of neuroscience. 2003;18:2769-2778.
7. Kriegstein A, Alvarez-Buylla A. The glial nature of embryonic and adult neural stem cells. Annual review of neuroscience. 2009;32:149-184.
8. Mignone JL, Kukekov V, Chiang AS, et al. Neural stem and progenitor cells in nestin-GFP transgenic mice. The Journal of comparative neurology. 2004;469:311-324.
9. Steiner B, Klempin F, Wang L, et al. Type-2 cells as link between glial and neuronal lineage in adult hippocampal neurogenesis. Glia. 2006;54:805-814.
10. Suh H, Consiglio A, Ray J, et al. In vivo fate analysis reveals the multipotent and self-renewal capacities of Sox2+ neural stem cells in the adult hippocampus. Cell stem cell. 2007;1:515-528.
11. Lugert S, Basak O, Knuckles P, et al. Quiescent and active hippocampal neural stem cells with distinct morphologies respond selectively to physiological and pathological stimuli and aging. Cell stem cell. 2010;6:445-456.
12. Noctor SC, Flint AC, Weissman TA, et al. Neurons derived from radial glial cells establish radial units in neocortex. Nature. 2001;409:714-720.
13. Shapiro LA, Korn MJ, Shan Z, et al. GFAP-expressing radial glia-like cell bodies are involved in a one-to-one relationship with doublecortin-immunolabeled newborn neurons in the adult dentate gyrus. Brain research. 2005;1040:81-91.

14. Bonaguidi MA, Wheeler MA, Shapiro JS, et al. In vivo clonal analysis reveals self-renewing and multipotent adult neural stem cell characteristics. Cell. 2011;145:1142-1155.
15. Gerald J. Sun YZ, Ryan P. Stadel, Jonathan Moss, Jing Hui A. Yong, Shiori Ito, Nicholas K. Kawasaki, Alexander T. Phaa, Justin H. Oh, Nikhil Modak, Randall R. Reed, Nicolas Toni, Hongjun Song, and Guo-li Ming. Tangential migration of neuronal precursors of glutamatergic neurons in the adult mammalian brain. PNAS. 2015.
16. Fuentealba LC, Obernier K, Alvarez-Buylla A. Adult neural stem cells bridge their niche. Cell stem cell. 2012;10:698-708.
17. Shihabuddin LS, Horner PJ, Ray J, et al. Adult spinal cord stem cells generate neurons after transplantation in the adult dentate gyrus. The Journal of neuroscience : the official journal of the Society for Neuroscience. 2000;20:8727-8735.
18. Palmer TD, Willhoite AR, Gage FH. Vascular niche for adult hippocampal neurogenesis. The Journal of comparative neurology. 2000;425:479-494.
19. Lie DC, Colamarino SA, Song HJ, et al. Wnt signalling regulates adult hippocampal neurogenesis. Nature. 2005;437:1370-1375.
20. Song H, Stevens CF, Gage FH. Astroglia induce neurogenesis from adult neural stem cells. Nature. 2002;417:39-44.
21. Song J, Zhong C, Bonaguidi MA, et al. Neuronal circuitry mechanism regulating adult quiescent neural stem-cell fate decision. Nature. 2012;489:150-154.
22. Gebara E, Sultan S, Kocher-Braissant J, et al. Adult hippocampal neurogenesis inversely correlates with microglia in conditions of voluntary running and aging. Frontiers in neuroscience. 2013;7:145.
23. Sierra A, Encinas JM, Deudero JJ, et al. Microglia shape adult hippocampal neurogenesis through apoptosis-coupled phagocytosis. Cell stem cell. 2010;7:483-495.
24. Ashton RS, Conway A, Pangarkar C, et al. Astrocytes regulate adult hippocampal neurogenesis through ephrin-B signaling. Nature neuroscience. 2012;15:1399-1406.
25. Nolte C, Matyash M, Pivneva T, et al. GFAP promoter-controlled EGFP-expressing transgenic mice: a tool to visualize astrocytes and astrogliosis in living brain tissue. Glia. 2001;33:72-86.
26. Yamaguchi M, Saito H, Suzuki M, et al. Visualization of neurogenesis in the central nervous system using nestin promoter-GFP transgenic mice. Neuroreport. 2000;11:1991-1996.
27. Madisen L, Zwingman TA, Sunkin SM, et al. A robust and high-throughput Cre reporting and characterization system for the whole mouse brain. Nature neuroscience. 2010;13:133-140.
28. Thuret S, Toni N, Aigner S, et al. Hippocampus-dependent learning is associated with adult neurogenesis in MRL/MpJ mice. Hippocampus. 2009;19:658-669.
29. Kuhn HG, Dickinson-Anson H, Gage FH. Neurogenesis in the dentate gyrus of the adult rat: age-related decrease of neuronal progenitor proliferation. The Journal of neuroscience : the official journal of the Society for Neuroscience. 1996;16:2027-2033.
30. Sultan S, Gebara EG, Moullec K, et al. D-serine increases adult hippocampal neurogenesis. Frontiers in neuroscience. 2013;7:155.
31. Villeda SA, Luo J, Mosher KI, et al. The ageing systemic milieu negatively regulates neurogenesis and cognitive function. Nature. 2011;477:90-94.
32. Monje ML, Toda H, Palmer TD. Inflammatory blockade restores adult hippocampal neurogenesis. Science. 2003;302:1760-1765.

33. Encinas JM, Michurina TV, Peunova N, et al. Division-coupled astrocytic differentiation and age-related depletion of neural stem cells in the adult hippocampus. Cell stem cell. 2011;8:566-579.
34. Filippov V, Kronenberg G, Pivneva T, et al. Subpopulation of nestin-expressing progenitor cells in the adult murine hippocampus shows electrophysiological and morphological characteristics of astrocytes. Molecular and cellular neurosciences. 2003;23:373-382.
35. Sierra A, Martin-Suarez S, Valcarcel-Martin R, et al. Neuronal hyperactivity accelerates depletion of neural stem cells and impairs hippocampal neurogenesis. Cell stem cell. 2015;16:488-503.

Figure legends

Figure 1: Morphometrical parameters of RGL cells
(A) Confocal maximal projection micrographs of type α and type β RGL cells in GFAP-GFP and Nestin-GFP mice. **(B)** Drawing of a RGL neural stem cell illustrating the measurements of length and width of the cell. **(C)** Scatter graph of all RGL cells analyzed morphometrically (n=2472 for GFAP-GFP mice and n=1150 for Nestin-GFP mice). **(D-E)** Schematic illustration (**D**) and histogram (**E**) of the projected surface of the dendritic arbor of secondary processes in type α and type β cells. **(F-G)** Schematic illustration **(F**) and histogram (**G**) of the position of the soma of type α and the type β cells relative to the hilar border of the granule cell layer. **(H-I)** Schematic illustration (**H**) and histogram (**I**) of the total surface of type α and type β cells. **(J-K)** Drawing (**J**) and histogram (**K**) of the number of branches of the main process of type α and the type β cells. Scale bar: 20 μm. Bilateral Student's t-test **p<0.01, ***p<0.001, NS: Not significant. Each value represents the mean ± SEM.

Figure 2: Molecular marker expression of type α and type β cells
(A) Confocal maximal projection micrographs of GFAP-GFP RGL cells (green), immunostained for Sox2. (**B**) Scatter graphs representing the dimensions of RGL cells immunostained for Sox2. **(C)** Confocal maximal projection micrographs of GFAP-GFP RGL cells (green), immunostained for GFAP. **(D)** Scatter graphs representing the dimensions of RGL cells immunostained for GFAP. **(E)** Confocal maximal projection micrographs of GFAP-GFP RGL cells (green), immunostained for Sox1. **(F)** Scatter graphs representing the dimensions of RGL cells immunostained for Sox1. **(G)** Confocal maximal projection micrographs of GFAP-GFP RGL cells (green), immunostained for Prominin1. **(H)** Scatter graphs representing the dimensions of RGL cells immunostained for Prominin1. **(I)** Confocal maximal projection micrographs of GFAP-GFP RGL cells (green), immunostained for Nestin. **(J)** Scatter graphs representing the dimensions of RGL cells immunostained for Nestin. **(K)** Confocal maximal projection micrographs of GFAP-GFP RGL cells (green), immunostained for S100β. **(L)** Scatter graphs representing the dimensions of RGL cells immunostained for S100β. **(M)** Confocal maximal projection micrographs of GFAP-GFP RGL cells (green), immunostained for GLT1. **(N)** Scatter graphs representing the dimensions of RGL cells immunostained for GLT1. Scale bars: 20 μm.

Figure 3: Type α and β cells contact niche-forming cells
(A) Experimental timeline. Mice were housed in normal cages (NR) or in cages containing a running wheel (R) for 2 weeks before histological analysis. **(B)** Confocal maximal projection micrographs of RGL cells (green) and Iba1-immunostained microglia (red). **(C)** Histogram of the average number of microglia cells contacted per RGL cell. Type β cells contact more microglia than type α cells (One-Way ANOVA $F(3, 15) = 73.12$; $p < 0.001$. Post-hoc bilateral Student's t-test: No Run [type α vs type β] $p < 0.001$, Run [type α vs type β] $p < 0.01$). Two

weeks of running decrease the interaction of microglia with both type α and type β cells (Post-hoc bilateral Student's t-test: type α [No Run vs Run] $p < 0.001$, type β [No Run vs Run] $p < 0.001$). **(D)** Confocal maximal projection micrographs of RGL cells (green) and blood vessels, identified with Sulforhodamine (red). **(E)** Histogram of the number of blood vessels contacted per RGL stem cell. In sedentary mice, there is no difference between type α of a type β cell in sedentary conditions (One-Way ANOVA $F(3, 15) = 16.10$; $p < 0.001$. Post-hoc bilateral Student's t-test: No Run [type α vs type β] $p = 0.84$). In running mice, blood vessel are more contacted by type α than type β cells (Post-hoc bilateral Student's t-test: Run [type α vs type β] $p < 0.05$). Running, significantly increased the number of blood vessels contacted by both cell types (One-Way ANOVA $F(3, 15) = 16.10$; $p < 0.001$. Post-hoc bilateral Student's t-test: type α [No Run vs Run] $p < 0.001$, type β [No Run vs Run] $p < 0.01$). **(F)** Confocal maximal projection micrographs of RGL cells (green) and S100β-immunostained astrocytes (white). **(G)** Histogram of the number of astrocytes contacted per type α or type β cells. **(H)** Confocal maximal projection micrographs of RGL cells (green) and NG2-immunostained oligodendrocyte precursors cells (red). **(I)** Histogram of the number of oligodendrocyte precursor cells contacted by type α or type β cells. NS: Not significant. Scale bars: 20 μm. N=4 animals per group. Each value represents the mean ± SEM. *p<0.05, **p<0.01, ***p<0.001, NS: Not significant.

Figure 4: Number of type α but not type β cells are changed by running and aging
(A) Experimental timeline. Mice were exposed to sedentary housing or cages with a running wheel (R), starting either at 42 days (Y) or 210 days (O) after birth. Mice were sacrificed and examined 2 weeks after exposure to running wheel cages. **(B)** Histogram of the total number of RGL cells in the dentate gyrus. Two-Way ANOVA test showed that there is interaction between aging and running [$F(1, 12) = 35.50$; $p < 0.001$]. The total number of RGL cells was significantly decreased with aging Post-hoc bilateral Student's t-test: Y vs. O $p < 0.001$] and increased by running [One-Way ANOVA $F(3, 15) = 127.32$; $p < 0.001$. Post-hoc bilateral Student's t-test: Y vs. YR $p < 0.001$, O vs. OR $p < 0.001$. **(C)** Histogram of the number of type α cells in the dentate gyrus. Voluntary running increased, whereas aging decreased the number of type α cells Kruskal-Wallis test $p < 0.01$. Post-hoc Wilcoxon test: Y vs. O < 0.05; Kruskal-Wallis test $p < 0.01$. Post-hoc Wilcoxon test: Y vs. YR $p < 0.05$, O vs. OR $p < 0.05$). **(D)** Histogram of the number of type β cells in the dentate gyrus. **(E)** Confocal maximal projection micrographs of hippocampal sections. Scale bars: 100 μm. *p<0.05, ***p<0.001, NS: Not significant.

Figure 5: Number of type α and type β cells are increased by D-serine injection
(A) Experimental timeline: Animals were injected with D-serine, daily for 8 days, starting at 49 days after birth and were sacrificed one day after the last D-serine injection. **(B)** Histogram of the total number of RGL cells in the dentate gyrus (bilateral Student's t-test $p < 0.001$). **(C)** Histogram of the number of type α cells in the dentate gyrus (bilateral Student's t-test $p < 0.001$). **(D)** Histogram of the number of the type β cells in the dentate gyrus (bilateral Student's t-test $p < 0.01$). **(E)** Confocal maximal projection micrographs of hippocampal sections. (**F**) Scatter graph of RGL cells dimensions. Red dots: Ki-67$^+$ cells N=45, black dots Ki-67$^-$ cells N=500. **(G)** Histogram showing the percentage of type α and type β cells expressing Ki-67. Bilateral Student's t-test. Scale bars: 100 μm. N= 4 animals per group. Each value represents the mean ± SEM. **p<0.01, ***p<0.001.

Figure 6: Proliferative properties of type α and type β cells
(A) Confocal maximal projection micrograph of RGL cell (green), immunostained for Ki-67 (red). **(B)** Scatter graph of RGL cell dimensions. Red dots: Ki-67$^+$ cells N=86, black dots Ki-

67$^-$ cells N=1469. **(C)** Histogram showing the percentage of type α and type β cells expressing Ki-67. Bilateral Student's t-test. **(D)** Line graph representing the proportion of RGL cells expressing Ki-67 according to their length. **(E)** Experimental timeline: mice were injected intraperitoneally at doses of 100 mg/kg in saline, 3 times at 2-h intervals and sacrificed 2 hours after the last injection. (**F**) Histogram showing the percentage of type α and type β cells expressing BrdU. N=500 cells. Bilateral Student's t-test. (**G**) Experimental timeline: mice were injected intraperitoneally at doses of 100 mg/kg in saline, 3 times at 2-h intervals and sacrificed 24 hours after the last injection. (**H**) Confocal maximal projection micrograph of type α and type β cells expressing BrdU. Confocal micrograph of one focal plan showing the immunoreactive cells Scale bar: 20 μm (**I**) Histogram showing the percentage of type α and type β cells expressing BrdU. N=500 cells. Bilateral Student's t-test. (**J**) Experimental timeline: Mice were injected daily with BrdU for 8 consecutive days, starting at 49 days after birth. One day after the last injection, they were sacrificed and prepared for histology. **(K)** Scatter graphs representing the dimensions of RGL cells after immunostaining for BrdU (red dots: BrdU$^+$ cells N=35, black dots BrdU$^-$ cells N=492) **(L)** Histogram showing the proportion of type α and type β cells that incorporated BrdU. Bilateral Student's t-test. Scale bar: 20 μm. Each value represents the mean ± SEM. **p<0.01 ***p<0.001.

Figure 7: Clonal analysis of type α and type β cells

(A) Breeding scheme for clonal analysis: Nestin-CreER^{T2} mice were crossed to fluorescent reporter mice Rosa-tdTomato or Z/EG$^{f/+}$ and GFAP::CreER^{T2} were crossed with ROSA-YFP reporter mice **(B)** Experimental timeline: mice were injected with tamoxifen (Tam) at 56 days after birth and sacrificed 1, 2, 3 and 7 day after Tam injection (dpi). **(C)** Venn diagram showing the percentage of clones that generated neurons, astrocytes or RGL cells out of all clones that divided. **(D)** Pie chart representing the distribution of newly generated RGL cells among clones that generated new RGL cells. **(E)** Histogram showing the percentage of newly generated RGL among the total number of dividing clones. **(F-H)** Confocal micrographs of different clones with hypothetic (linkage) tree of fate. Clones generated either only new RGL cells (**F**), neuronal progenitor/type 2 cell (**G**) or astrocytes (**H**). (N= type 2/neuronal progenitor, A= astrocyte). Scale bars: 20 μm.

Supplementary Figure 1: Morphological and molecular characterization of type α and type β cells

(**A**) Table of the morphological parameters of type α and type β in both GFAP-GFP and Nestin-GFP mice. Data are the mean value ± SEM. (**B**) Table of the percentage of marker expression in type α and type β cells. In red: Number of cells analyzed.

Supplementary Figure 2: Effect of running on microglia and blood vessels

(**A**) Histogram of the number of Iba1$^+$ cells per dentate gyrus. Bilateral Student's t-test. (**B**) Histogram of the territory area occupied by microglial cells. Bilateral Student's t-test. (**C**) Histogram of the number of branches per microglial cell. Bilateral Student's t-test. (**D**) Confocal maximal projection micrographs of dentate gyrus stained for blood vessels. (**E**) Line graph of the number of pixels per fluorescence intensity of blood vessels in young and young runner mice. (**F**) Histogram of the fluorescence intensity of the peak number of pixels of blood vessels. Bilateral Student's t-test. **p<0.01. ***p<0.001. Scale bar: 100 μm.

Supplementary Figure 3: Effect of running or aging the morphology of type α and type β cells:

(A-D) Scatter graphs representing the dimensions of RGL cells in young mice (**A**), young mice exposed to running wheel (**B**), old mice (**C**) and old mice exposed to running wheel (**D**).

Supplementary Figure 4: Clonal analysis of type α and type β cells
(A) Pie charts of the quantitative comparison of the frequency of division (No division, one or two divisions), and the frequency of different clone types (α, α-α, α-β, α-N, α-α-N, α-β-N, α-A, β-A α-α-A, α-β-A, β-β-A) at 1, 2, 3,7dpi and all time points in Nestin::CreER^{T2} mice **(B)** Pie charts of the quantitative comparison of the frequency of division (No division, one or two divisions), and the frequency of different clone types (α, α-α, α-β, α-N, α-α-N, α-β-N, α-A, β-A α-α-A, α-β-A, β-β-A) at 1,7dpi and all time points in GFAP::CreER^{T2} mice.

Supplementary Figure 5: Clones containing type α and type β cells
(**A**-**B**) Table representing all clones analyzed in Nestin-GFP mice (**A**) and in GFAP-GFP mice (**B**). Numbers indicate number of clones analyzed and in brackets are the proportion of each clone.

Supplementary Figure 6: Identification of clones and progenies
(**A**) Confocal micrograph of type α cell with a GFAP$^-$/type 2 neural progenitor cell (N). (**B**) Confocal micrograph of type α cell with a GFAP$^+$/astrocyte. (**C**) Confocal micrograph of 2 type α cells with a GFAP$^+$/astrocyte. (**D**) Low magnification confocal micrograph of Nestin Cre::ER^{T2}-td-tomato mouse (left) and a GFAP Cre::ER^{T2}-ROSA-YFP mouse (right). Scale bars: 20 μm (panels A-C) and 100 μm (panels D, E).

Supplementary Figure 7: Model of type α and type β cells lineage relationship
Model of the lineage relationship of type α and type β cells in the adult mouse hippocampus under basal conditions. Type α cells can self-renew (1) and also generate type 2 neural progenitors (2), type β cells (3) and astrocytes (4). Type β cells do not divide, but may revert to type α cell (??) or transform into astrocytes (5). Also shown are marker expression.

Graphical abstract: Model of type α and type β cells lineage relationship
Model of the lineage relationship of type α and type β cells in the adult mouse hippocampus under basal conditions. Type α cells can self-renew (1) and also generate type 2 neural progenitors (2), type β cells (3) and astrocytes (4). Type β cells do not divide, but may revert to type α cell (??) or transform into astrocytes (5). Also shown are marker expression.

Figure 1

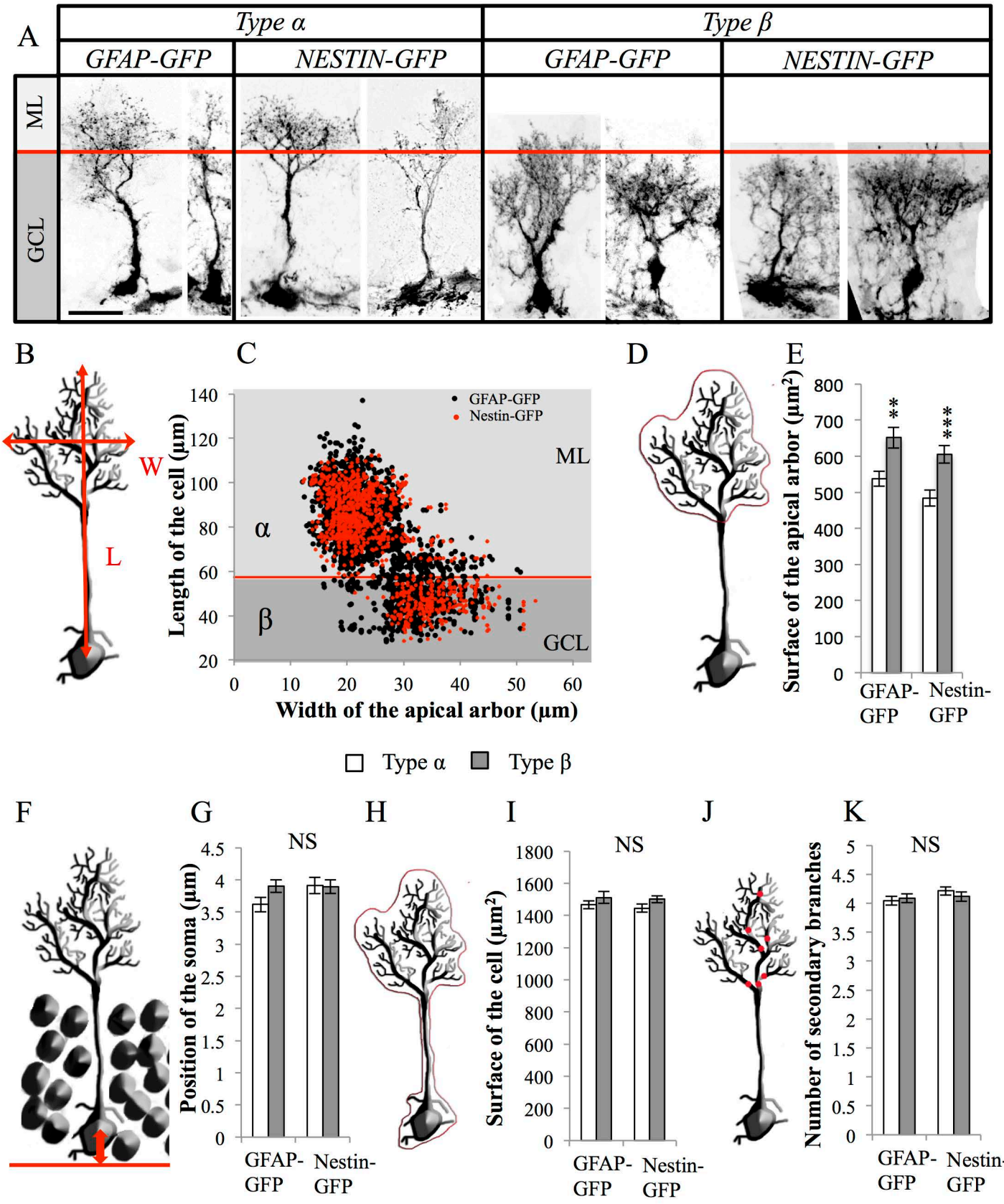
A
Type α
Type β
GFAP-GFP
NESTIN-GFP
GFAP-GFP
NESTIN-GFP
ML
GCL
B
W
L
C
GFAP-GFP
Nestin-GFP
ML
GCL
α
β
Length of the cell (µm)
Width of the apical arbor (µm)
D
E
Surface of the apical arbor (µm²)
**
***
GFAP-GFP
Nestin-GFP
Type α
Type β
F
G
NS
Position of the soma (µm)
GFAP-GFP
Nestin-GFP
H
I
NS
Surface of the cell (µm²)
GFAP-GFP
Nestin-GFP
J
K
NS
Number of secondary branches
GFAP-GFP
Nestin-GFP

Figure 2

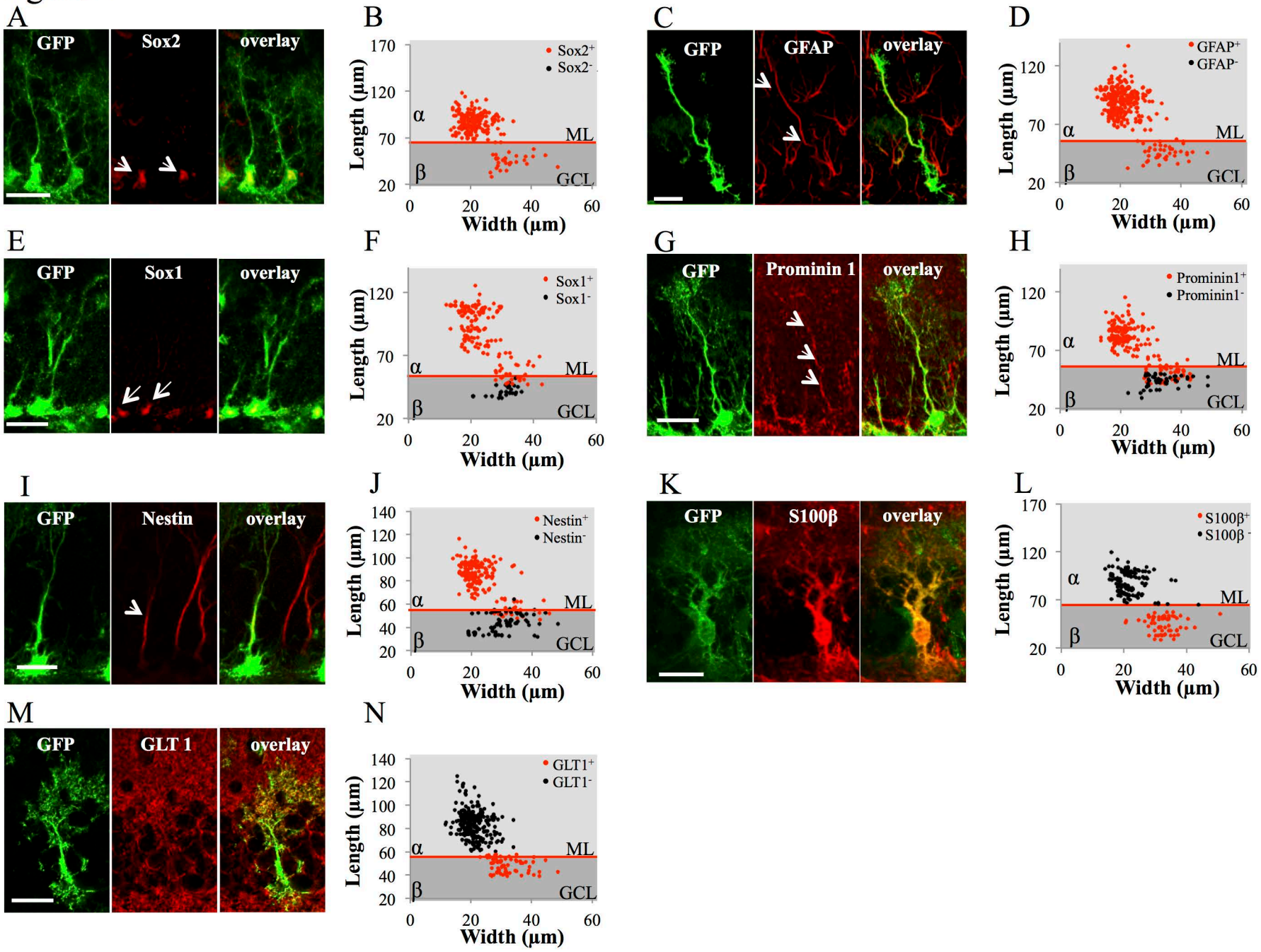
A
GFP
Sox2
overlay
B
Sox2+
Sox2-
Length (µm)
Width (µm)
α
β
ML
GCL
C
GFP
GFAP
overlay
D
GFAP+
GFAP-
E
GFP
Sox1
overlay
F
Sox1+
Sox1-
G
GFP
Prominin 1
overlay
H
Prominin1+
Prominin1-
I
GFP
Nestin
overlay
J
Nestin+
Nestin-
K
GFP
S100β
overlay
L
S100β+
S100β -
M
GFP
GLT 1
overlay
N
GLT1+
GLT1-

Figure 3

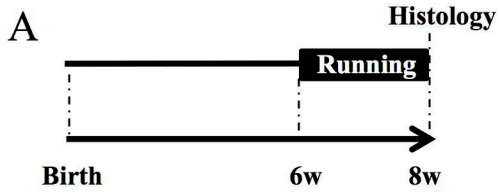
A
Histology
Running
Birth
6w
8w

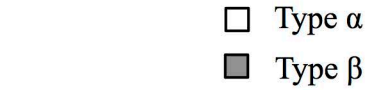
Type α
Type β

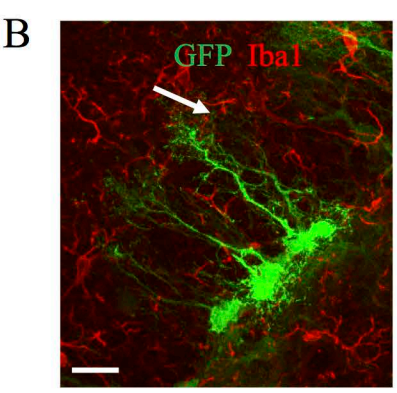
B
GFP Iba1

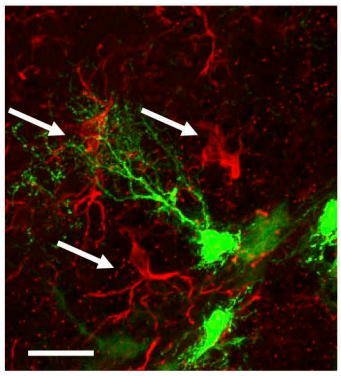

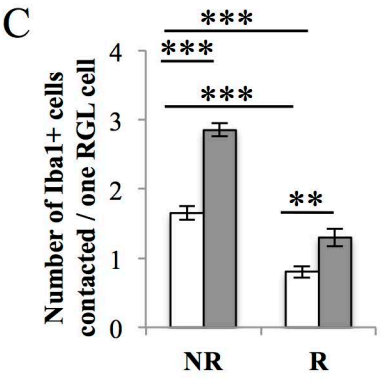
C
***
***
***
**
Number of Iba1+ cells contacted / one RGL cell
4
3
2
1
0
NR
R

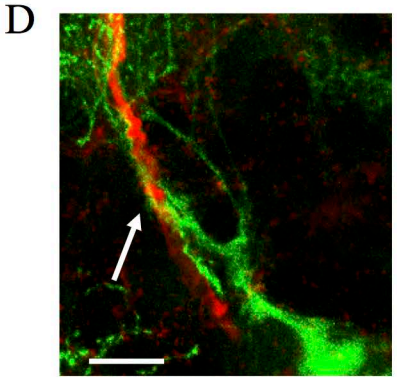
D

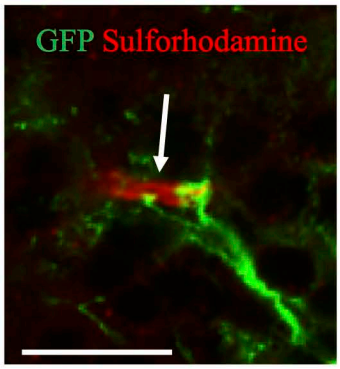
GFP Sulforhodamine

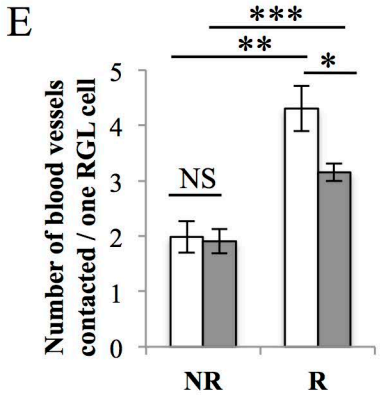
E
***
**
*
NS
Number of blood vessels contacted / one RGL cell
5
4
3
2
1
0
NR
R

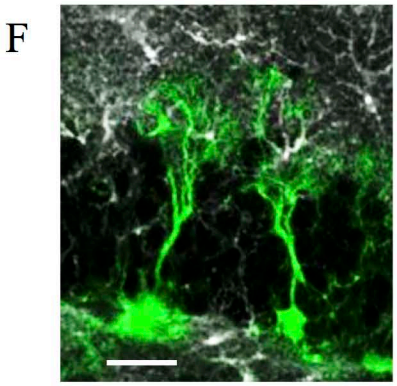
F

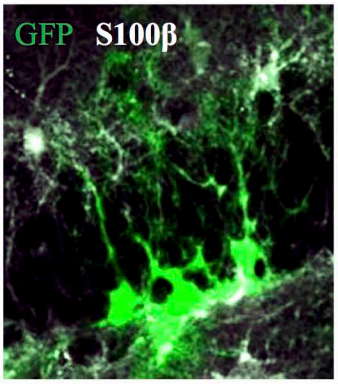
GFP S100β

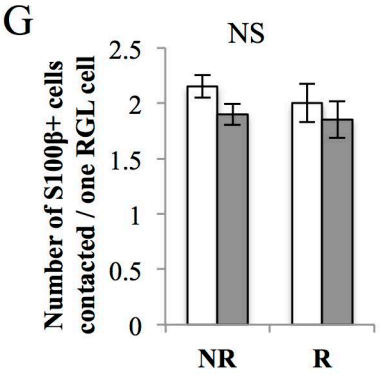
G
NS
Number of S100β+ cells contacted / one RGL cell
2.5
2
1.5
1
0.5
0
NR
R

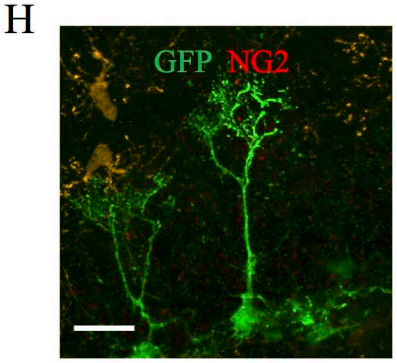
H
GFP NG2

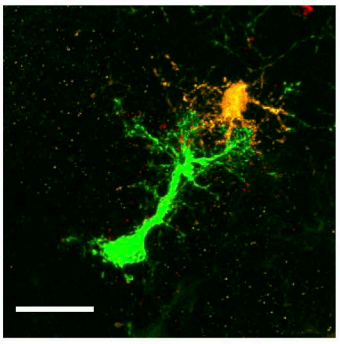

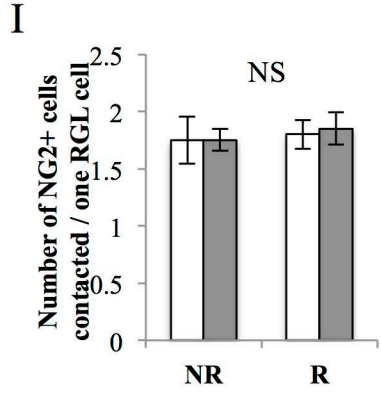
I
NS
Number of NG2+ cells contacted / one RGL cell
2.5
2
1.5
1
0.5
0
NR
R

Figure 4

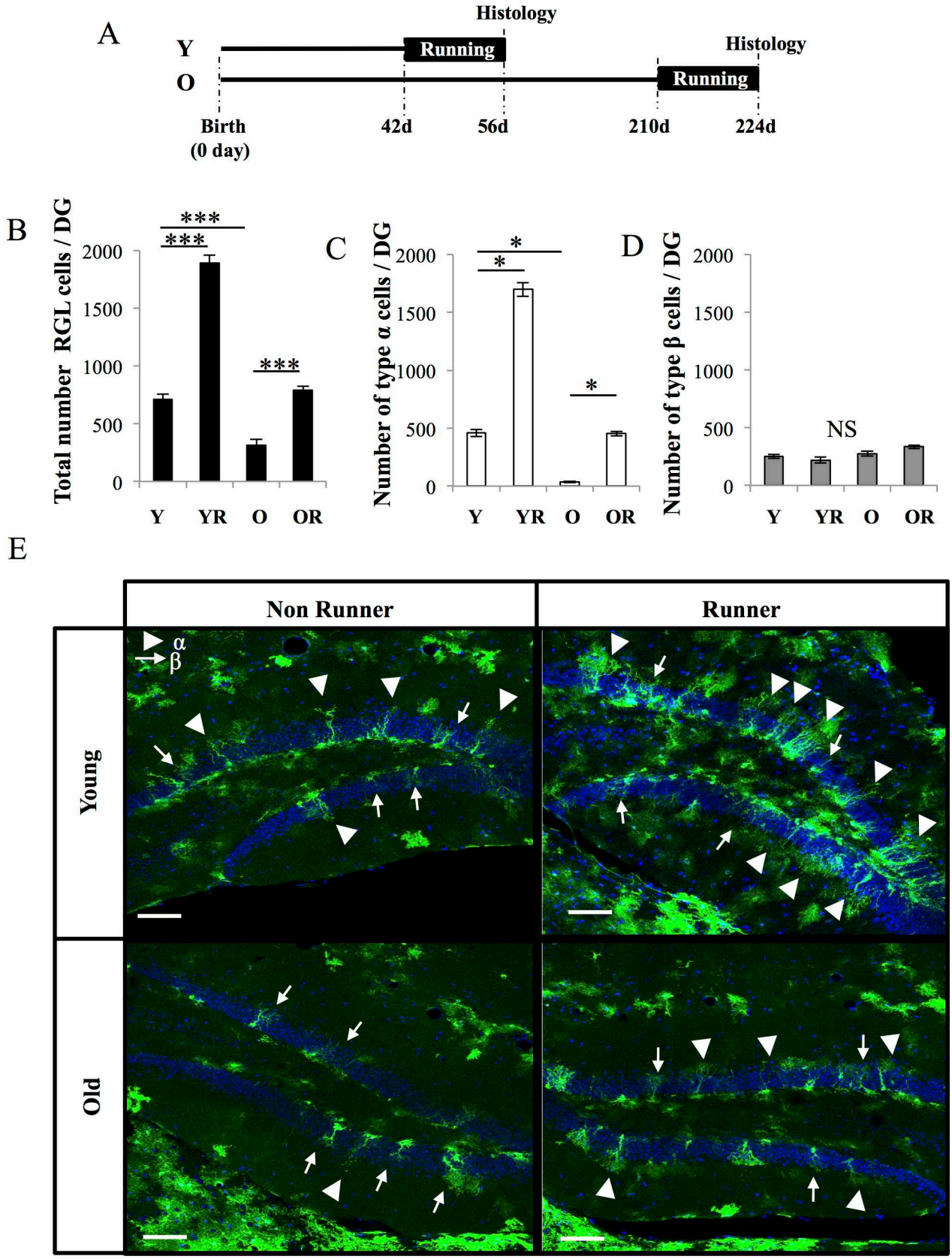
A
Histology
Y
Running
Histology
O
Running
Birth
(0 day)
42d
56d
210d
224d
B
Total number RGL cells / DG
***
***
***
2000
1500
1000
500
0
Y
YR
O
OR
C
Number of type α cells / DG
*
*
*
2000
1500
1000
500
0
Y
YR
O
OR
D
Number of type β cells / DG
NS
2000
1500
1000
500
0
Y
YR
O
OR
E
Non Runner
Runner
Young
Old
α
β

Figure 5

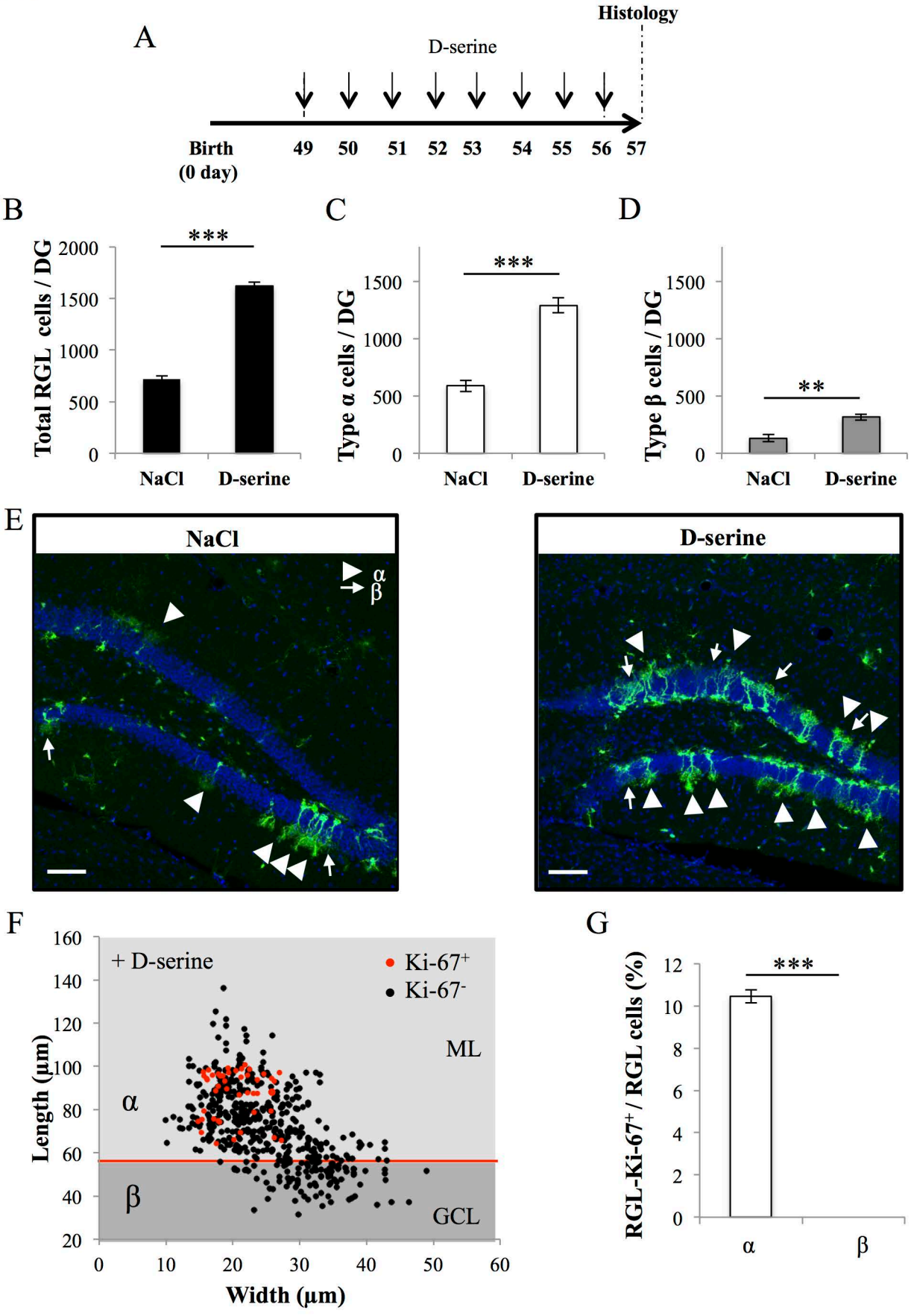
A
Histology
D-serine
Birth
(0 day)
49
50
51
52
53
54
55
56
57
B
Total RGL cells / DG
***
NaCl
D-serine
C
Type α cells / DG
***
NaCl
D-serine
D
Type β cells / DG
**
NaCl
D-serine
E
NaCl
D-serine
α
β
F
+ D-serine
Ki-67+
Ki-67-
ML
GCL
α
β
Length (μm)
Width (μm)
G
RGL-Ki-67+ / RGL cells (%)
***
α
β

Figure 6

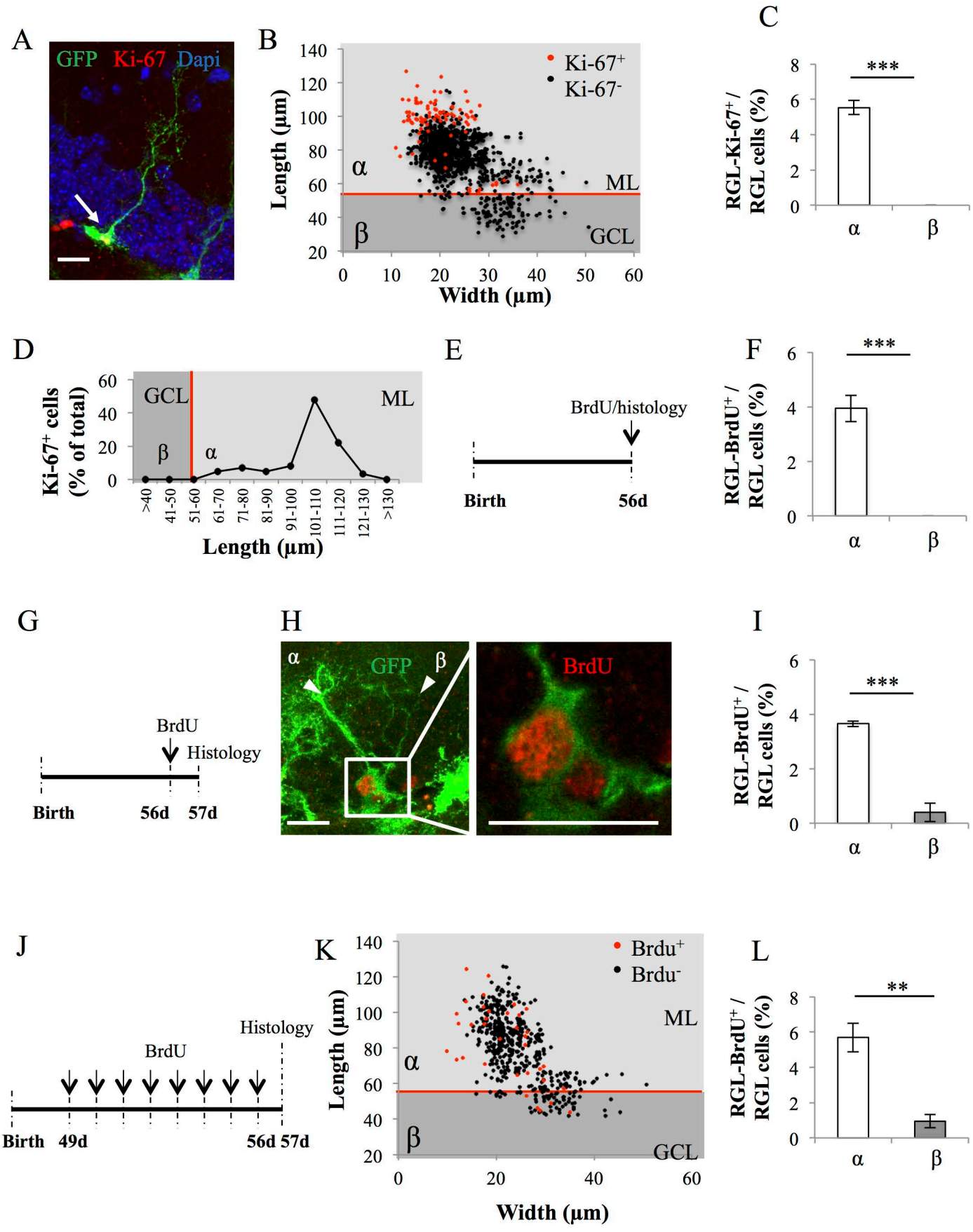
A
GFP Ki-67 Dapi
B
Ki-67+
Ki-67-
Length (µm)
Width (µm)
α
β
ML
GCL
C
RGL-Ki-67+ / RGL cells (%)
***
α
β
D
Ki-67+ cells (% of total)
GCL
ML
Length (µm)
E
BrdU/histology
Birth
56d
F
RGL-BrdU+ / RGL cells (%)
***
G
BrdU
Histology
Birth
56d
57d
H
GFP
BrdU
I
RGL-BrdU+ / RGL cells (%)
***
J
BrdU
Histology
Birth
49d
56d 57d
K
Brdu+
Brdu-
Length (µm)
Width (µm)
L
RGL-BrdU+ / RGL cells (%)
**

Figure 7

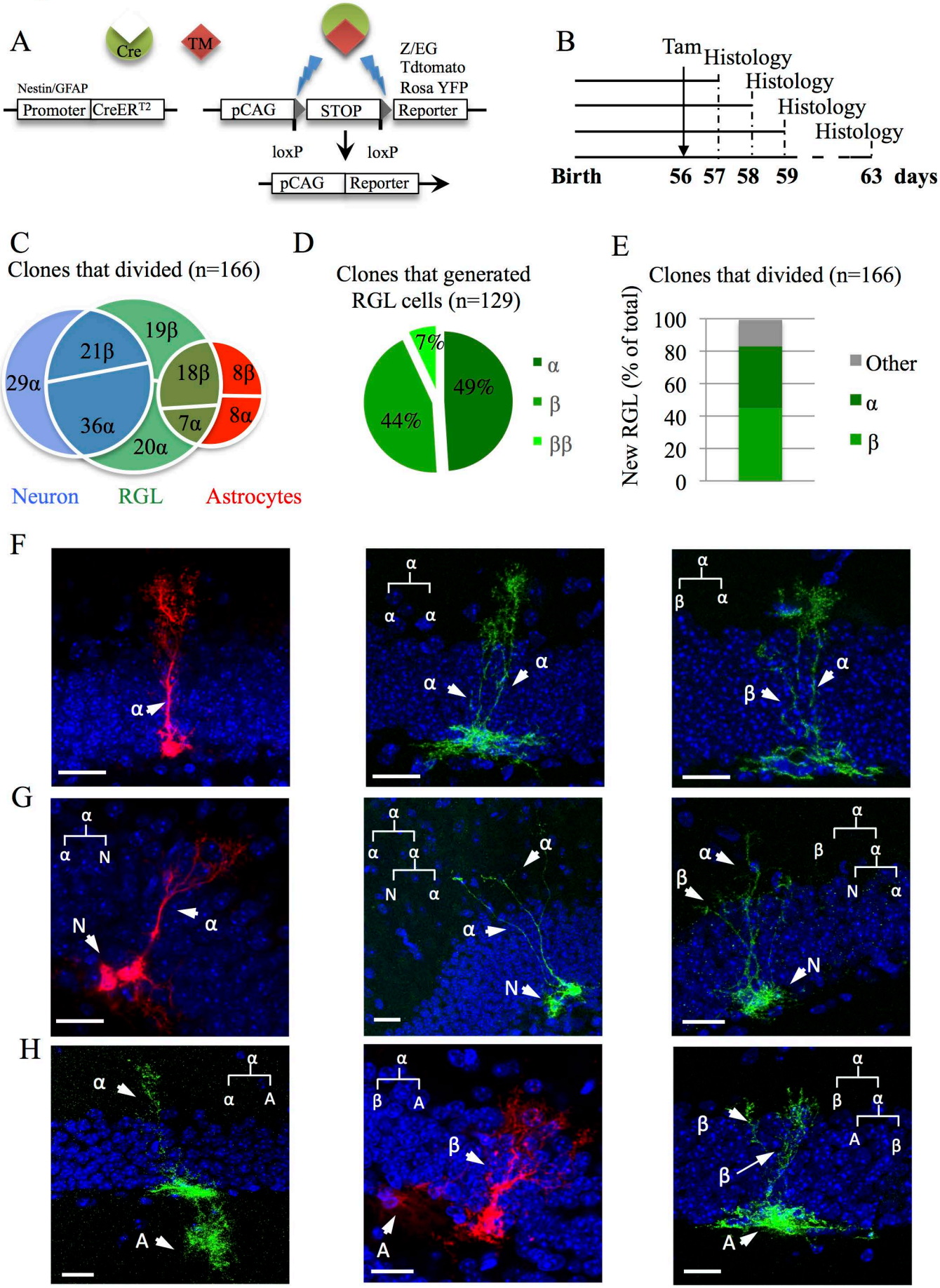
A
Cre
TM
Nestin/GFAP
Promoter
CreER^{T2}
pCAG
STOP
Reporter
Z/EG
Tdtomato
Rosa YFP
loxP
loxP
pCAG
Reporter
B
Tam
Histology
Histology
Histology
Histology
Birth
56
57
58
59
63 days
C
Clones that divided (n=166)
29α
21β
19β
18β
8β
36α
7α
8α
20α
Neuron
RGL
Astrocytes
D
Clones that generated RGL cells (n=129)
7%
49%
44%
α
β
ββ
E
Clones that divided (n=166)
New RGL (% of total)
100
80
60
40
20
0
Other
α
β
F
G
H
α
β
N
A

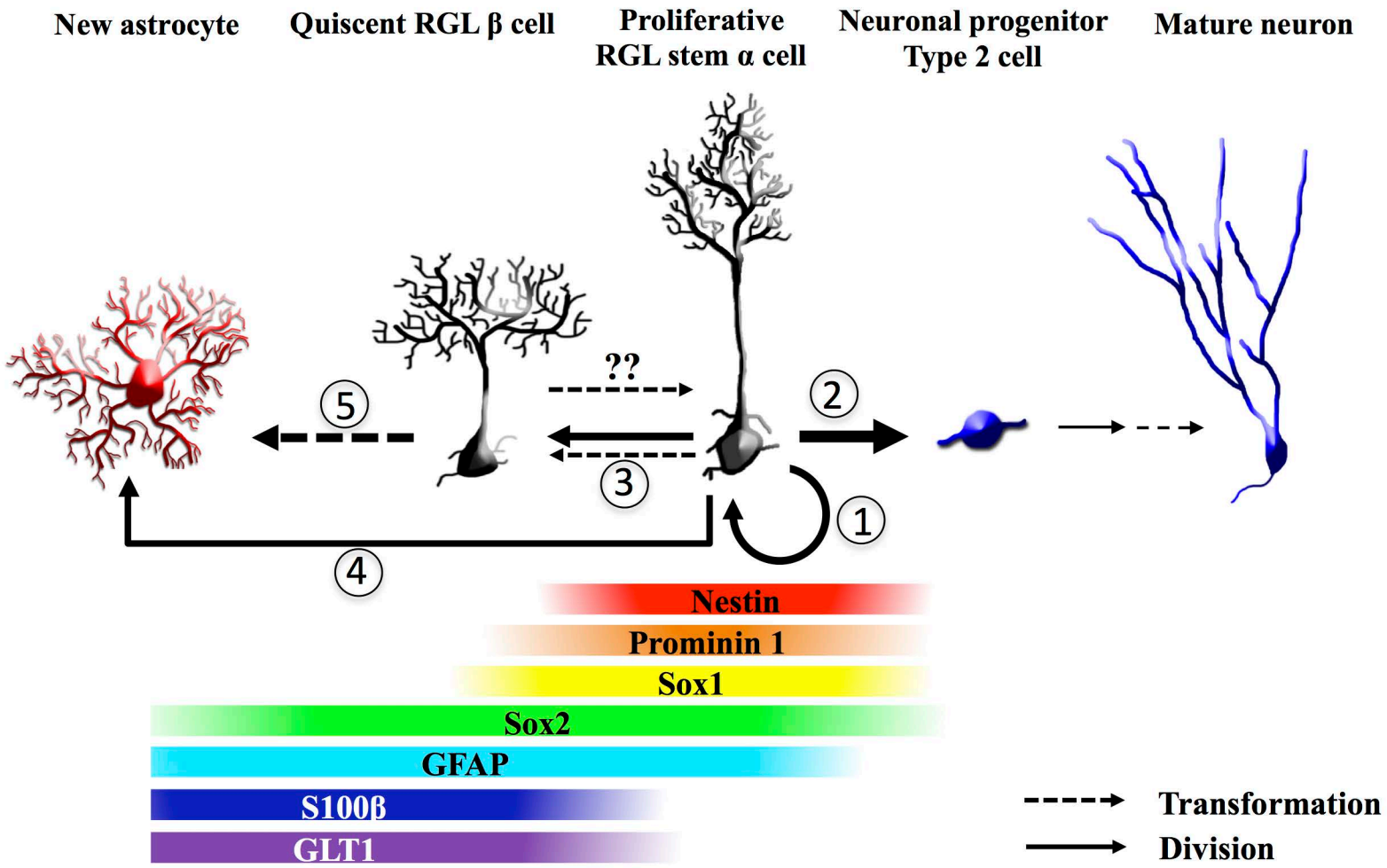
New astrocyte
Quiscent RGL β cell
Proliferative
RGL stem α cell
Neuronal progenitor
Type 2 cell
Mature neuron
??
1
2
3
4
5
Nestin
Prominin 1
Sox1
Sox2
GFAP
S100β
GLT1
Transformation
Division

Supplementary figure 1

A

	GFAP-GFP		Nestin-GFP	
	α	β	α	β
Width of the apical arbor	22.63 ± 0.11 (n=1884)	32.45 ± 0.23 (n=588)	22.00 ± 0.17 (n=849)	35.37 ± 0.32 (n=301)
Length of the cell	84.64 ± 0.29 (n=1884)	46.02 ± 0.27 (n=588)	87.59 ± 0.39 (n=849)	45.69 ± 0.36 (n=301)
Surface of the apical arbor	537.89 ± 21.10 (n=110)	651.33 ± 28.84 (n=110)	483.88 ± 22.15 (n=110)	604.93 ± 24.33 (n=110)
Position of the soma	3.61 ± 0.11 (n=500)	3.91 ± 0.12 (n=500)	3.90 ± 0.10 (n=500)	3.89 ± 0.10 (n=500)
Surface of the cell	1466.16 ± 24.02 (n= 300)	1444.66 ± 25.68 (n= 300)	1511.60 ± 35.98 (n=300)	1501.00 ± 22.07 (n=300)
Number of secondary branches	4.04 ± 0.076 (n= 500)	4.21 ±0.073 (n=500)	4.09 ± 0.077 (n=500)	4.11 ± 0.081 (n=500)

B

	Type α	Type β
Sox2	100% (n=165)	100% (n=62)
GFAP	100% (n=253)	100% (n=97)
Sox1	100% (n=166)	49% (n=52)
Prominin 1	100% (n=168)	32% (n=75)
Nestin	100% (n= 174)	18% (n= 75)
S100β	0.5% (n= 134)	100% (n=52)
Glt1	0% (n=248)	100% (n=69)

Supplementary figure 2

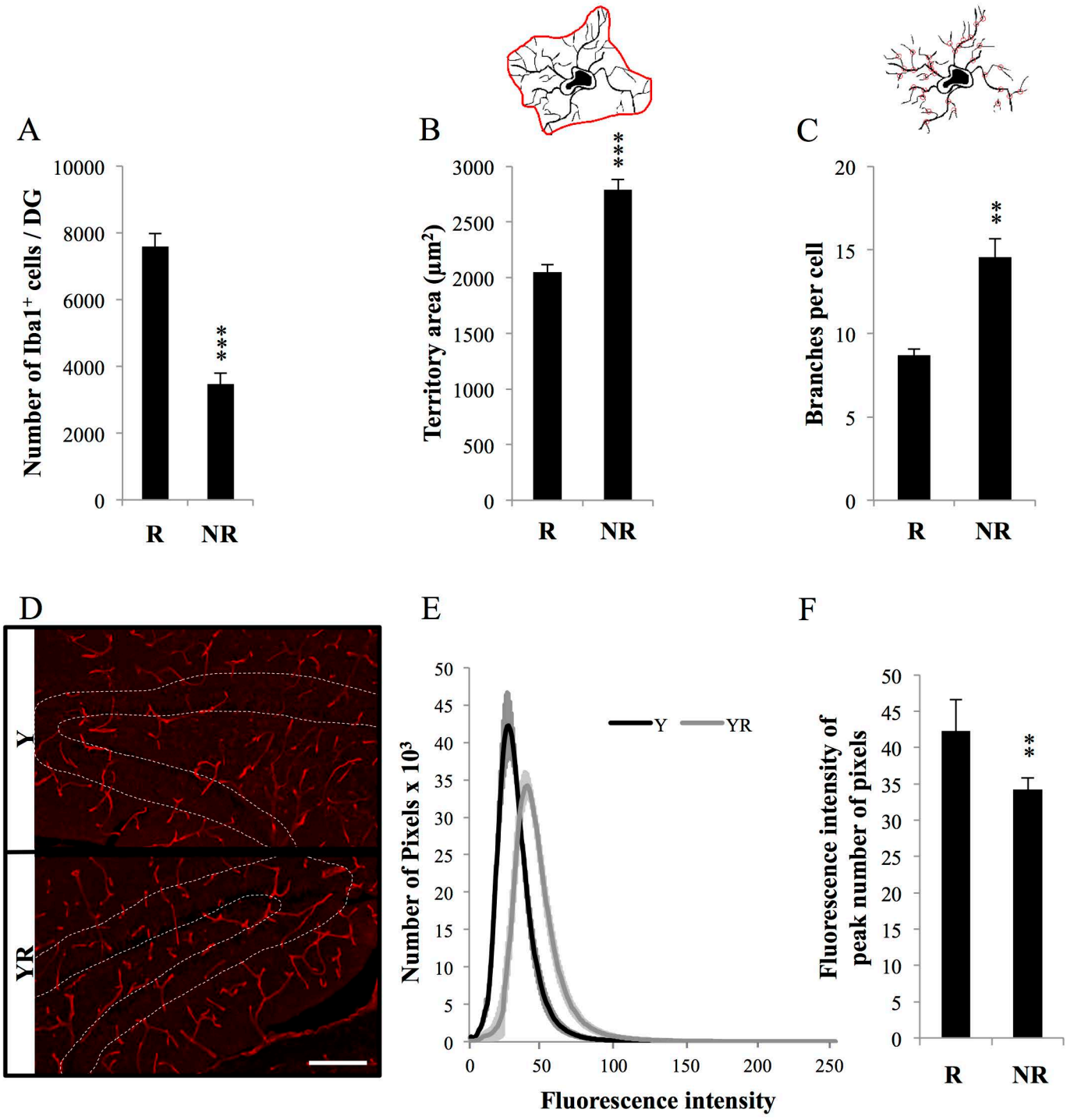

Supplementary figure 3

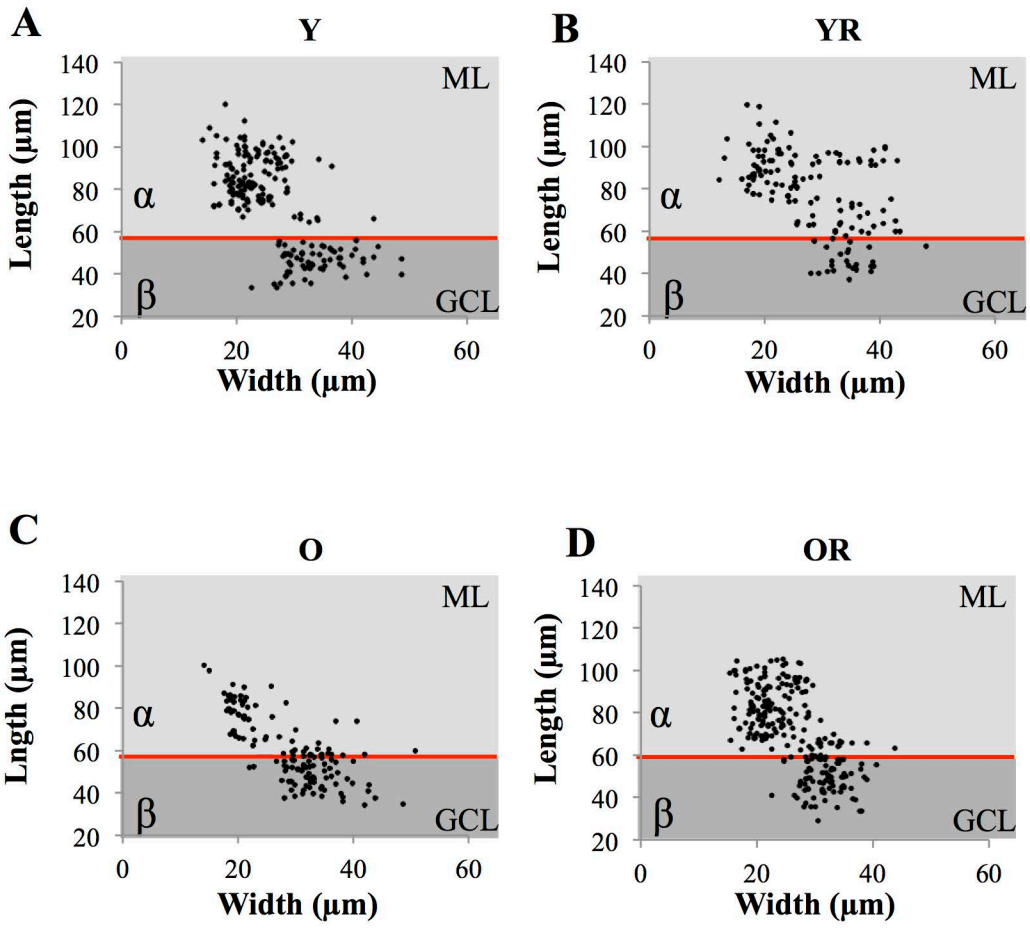

Supplementary figure 4

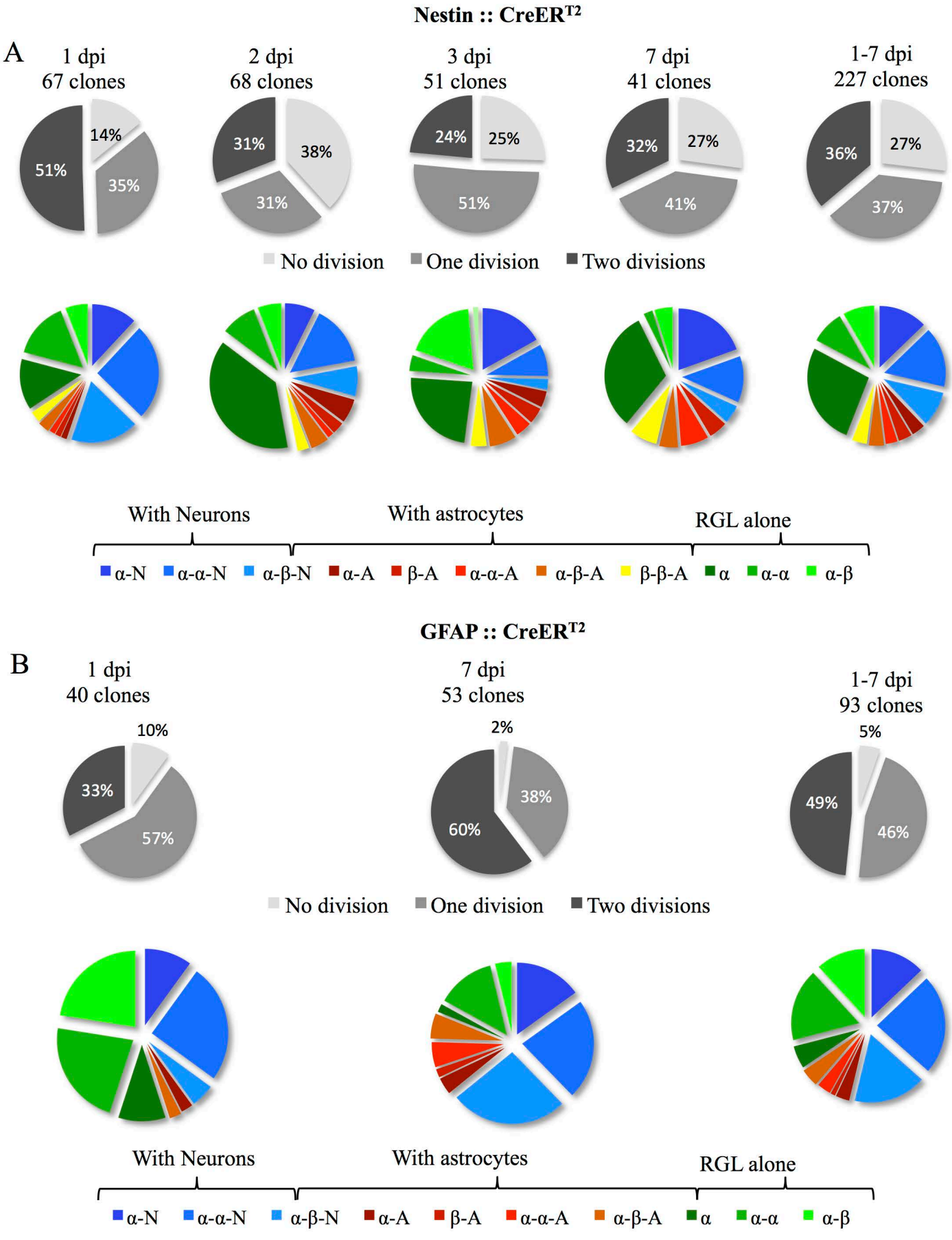

Supplementary figure 5

A

Nestin :: CreER^{T2}

	α-N	β-N	α-α-N	α-β-N	β-β-N	α-A	β-A	α-α-A	α-β-A	β-β-A	α	β	α-α	α-β	β-β
Dpi															
1	8 (3.52 %)	0	17 (7.49 %)	12 (5.29 %)	0	1 (0.44 %)	1 (0.44 %)	1 (0.44 %)	2 (0.88 %)	2 (0.88 %)	9 (3.96 %)	0	10 (4.41 %)	4 (1.76 %)	0
2	5 (2.20 %)	0	10 (4.41 %)	5 (2.20 %)	0	4 (1.76 %)	2 (0.88 %)	1 (0.44 %)	3 (1.32 %)	2 (0.88 %)	26 (11.45 %)	0	6 (2.64 %)	4 (1.76 %)	0
3	8 (3.52 %)	0	4 (1.76 %)	2 (0.88 %)	0	3 (1.32 %)	3 1.32	2 (0.88 %)	2 (0.88 %)	2 (0.88 %)	13 (5.73 %)	0	3 (1.32 %)	9 (3.96 %)	0
7	8 (3.52 %)	0	5 (2.20 %)	2 (0.88 %)	0	0	2 (0.88 %)	3 (1.32 %)	2 (0.88 %)	3 (1.32 %)	13 (5.73 %)	0	1 (0.44 %)	2 (0.88 %)	0
all	29 (12.78 %)	0	36 (15.86 %)	21 (9.25 %)	0	8 (3.52 %)	8 (3.52 %)	7 (3.08 %)	9 (3.96 %)	9 (3.96 %)	61 (26.87%)	0	20 (8.81 %)	19 (8.37 %)	0

B

GFAP :: CreER^{T2}

	α-N	β-N	α-α-N	α-β-N	β-β-N	α-A	β-A	α-α-A	α-β-A	β-β-A	α	β	α-α	α-β	β-β
Dpi															
1	4 (4.30 %)	0	10 (10.75 %)	2 (2.15 %)	0	1 (1.08 %)	0	0	1 (1.08 %)	0	4 (4.30 %)	0	9 (9.68 %)	9 (9.68 %)	0
7	8 (8.60 %)	0	12 (12.90 %)	14 (15.05 %)	0	1 (1.08 %)	1 (1.08 %)	2 (2.15 %)	5 (3.23 %)	0	1 (1.08 %)	0	7 (7.53 %)	2 (2.15 %)	0
all	12 (12.90 %)	0	22 (23.66 %)	16 (17.20 %)	0	2 (2.15 %)	1 (1.08 %)	2 (2.15 %)	6 (6.46 %)	0	5 (5.38 %)	0	16 (17.20 %)	11 (11.83%)	0

Supplementary figure 6